

GENERATION OF ULTRA-PACKED THERMAL GREASES AND
EVALUATION OF THEIR EFFECTIVE PROPERTIES

A Thesis

Submitted to the Faculty

of

Purdue University

by

Sukshitha Achar, Puttur Lakshminarayana

In Partial Fulfillment of the

Requirements for the Degree

of

Master of Science

December 2018

Purdue University

West Lafayette, Indiana

THE PURDUE UNIVERSITY GRADUATE SCHOOL
STATEMENT OF THESIS APPROVAL

Dr. Ganesh Subbarayan, Professor

School of Mechanical Engineering

Dr. Amy Marconnet

School of Mechanical Engineering

Dr. Justin Weibel

School of Mechanical Engineering

Approved by:

Dr. Anil. K. Bajaj

Head of the Mechanical Engineering

To the almighty. To my dearest family.

ACKNOWLEDGMENTS

I would like to acknowledge and sincerely thank Prof. Dr. Ganesh Subbarayan for his constant support. Working with him has been an absolute pleasure and I feel truly privileged to have been his student. His thorough academic expertise and patient mentoring has inspired me to be a humble and diligent learner. I would also like to thank the endearing support of my family. I would like to extend my gratitude to my fellow group members of the HiDAC lab for their guidance.

I would also like to acknowledge Cooling Technologies Research Consortium at Purdue University (CTRC) for supporting this research.

TABLE OF CONTENTS

	Page
LIST OF TABLES	vii
LIST OF FIGURES	viii
ABSTRACT	x
1 Introduction	1
1.1 Functionality of TIMs	1
1.2 Thermal Greases and their Modeling	3
1.3 Modeling Effective Behavior of TIMs	3
1.4 Microstructure Generation	3
1.5 Evaluation of Effective Properties	4
2 Evaluation of Effective Properties of Particulate Composites	5
2.1 Classical Models to Evaluate Effective Behavior of Composite Materials	5
2.1.1 Maxwell's Model	5
2.1.2 Rayleigh Model	7
2.1.3 Hasselman-Johnson Model	8
2.1.4 Bruggeman's Asymmetric Model	9
2.2 Percolation Based Models	9
2.3 Full-field Meshless Simulations	10
3 Random Network Model	13
3.1 Development of RNM	14
3.1.1 Validation of Random Network Model	16
3.2 Estimation of Effective Elastic Modulus Using Random Network Model	18
3.3 Extension of RNM for Modified Microstructures	21
3.3.1 Derivation of Limits for Inter-particle Conductance	21

	Page
3.4 Extension of Derivation for Cut Particles Along Edges	23
4 Comparative Evaluation of Algorithms for Microstructure Generation	26
4.1 Optimization Techniques to Generate Microstructures	27
4.1.1 Exterior Penalty Method	28
4.1.2 Sequential Quadratic Programming Algorithm	31
4.1.3 Conjugate Gradient Method	33
4.1.4 Augmented Lagrangian Method	36
4.1.5 Summary of Optimization Techniques	38
4.2 Heuristic Algorithm: Drop-Fall-Shake	39
4.2.1 Description of the Cells Method:	40
4.3 Summary of Comparative Algorithm Evaluations	41
5 Development of Algorithms for Generating Ultrapacked Microstructures . . .	43
5.1 Drop-Fall-Mix	43
5.2 Modified-Drop-Fall-Shake	45
5.3 Modified-Drop-Fall-Shake with RVE	47
5.4 Summary of Algorithms to Develop Ultrapacked Microstructures	49
5.5 Evaluation of Effective Properties of Ultrapacked Microstructures . . .	49
6 Conclusions and Future Work	54
6.1 Conclusions	54
6.2 Future Work	55
REFERENCES	56

LIST OF TABLES

Table	Page
4.1 Design variables and constraints	29
4.2 Summary of optimization techniques	38
5.1 Summary of Random Sequential Addition based Algorithms	49

LIST OF FIGURES

Figure	Page
1.1 Presence of interstitial air gaps between contact surfaces	2
1.2 Conforming TIMs reduce the interstitial air gaps between contact surfaces and decrease thermal resistance	2
2.1 Particle of radius a in infinite medium	7
2.2 Regular arrangement of spheres in a simple cube	8
2.3 Percolation: Formation of continuous chain of highly conducting particles (Devpura et al. [17])	10
2.4 Constructive modeling strategy that enables hierarchical operations on geometry, analysis fields and materials (source: Zhang et al. [19]).	11
2.5 (a) Temperature and (b) heat flux fields obtained at the midplane of the (c) microstructure ($y = 0.5$) using jNURBS.(source: Kanuparthi et al. [20]).	12
3.1 Network of resistors (source: Kanuparthi [10])	14
3.2 Cylindrical zone of heat transfer (source: Kanuparthi [10])	15
3.3 Semi-spherical zone of heat transfer in the fillers (source: Vaitheeswaran et al. [21])	17
3.4 Experimental effective thermal conductivity of samples (source: Kanu- parthi [10])	17
3.5 Comparison of numerical simulations with experimental results of (a) alumina fillers in silicone matrix (b) aluminum fillers in silicone matrix (source: Kanuparthi [10])	19
3.6 Comparison of RNM results with Full-field simulations (source: Kanu- parthi [10])	20
3.7 Force transfer across the matrix layer (source: Vaitheeswaran et al. [21]) .	20
3.8 Network of resistors in the RVE	22
3.9 Integrating a strip of length dx across the x - axis	22
3.10 Integration limits for the semi-spherical zone of conductance	23
3.11 Semi-spherical model for cut particles	24

Figure	Page
3.12 Modified particle conductance (a) integration of the strip from center of the particle to the edge (b)conductance of the cut particle	25
4.1 Optimization technique to pack spheres in a cube	27
4.2 Microstructure generated with exterior penalty method	31
4.3 Microstructure generated with sequential quadratic programming method	32
4.4 Microstructure generated with ALM (a) in a spherical container (b) in a cubic container	37
4.5 Schematic representation of Drop-Fall-Shake method.(Source: Zhang. X et al. [19] Smith, LN and Midha, PS [33])	40
4.6 Cells method to detect overlap only between neighboring particles. (a) cell 1 stores particles p0 and p2 (b) subdivision of 3D microstructures into cells	41
5.1 Ross Planetary Mixer (source: [34])	44
5.2 Schematic representation of Drop-Fall-Mix procedure	45
5.3 Microstructure generated with Drop-Fall-Mix method	46
5.4 Modified Drop-Fall-Shake method (a) original Drop-Fall-Shake method (b)modification to allow higher probability to move along x and y directions	47
5.5 Microstructure generated using the modified Drop-Fall-Shake method	47
5.6 Presence of gaps along the edges of the microstructure	48
5.7 RVE generated by cutting particles across the edges	48
5.8 Variation of Effective Properties (a) Effective Conductivity (b)Effective Elastic Modulus	51
5.9 Variation of Effective Properties with volume fraction. Five random microstructures were generated at each volume fraction (a) Effective Conductivity (b)Effective Elastic Modulus	52
5.10 Variation of effective properties with polydispersity (a) effective conductivity (b)effective elastic modulus	53
6.1 Microstructures generated with various algorithms	54

ABSTRACT

Puttur Lakshminarayana, Sukshitha Achar M.S, Purdue University, December 2018. Generation of Ultra-packed Thermal Greases and Evaluation of their Effective Properties. Major Professor: Ganesh Subbarayan.

Thermal Greases are gap-filling interface materials that are used in semiconductor packages to efficiently transfer heat from the component to the heat sink or spreader. Thermal greases are typically particle filled composite materials comprising of highly conducting fillers in a poorly conducting, but mechanically soft, silicone or epoxy base matrix. Generally, the effective conductivity of the greases increases with increasing volume fractions of fillers. However, the fillers also have high elastic modulus that induces undesirable thermal stresses on the brittle silicon device. Therefore, as device power density increases, there is a need to increase particle volume loading, which in turn necessitates optimally balancing the material's thermal and mechanical characteristics.

In this thesis, procedures are developed to simulate packed microstructures of particles so as to identify the optimal trade-off between thermal and mechanical behavior. Experimental and numerical simulations of microstructures that have been generated as reported in the literature were found to have volume fractions of around 60%. However, as commercially available thermal greases have volume fractions in the range of 60 – 80%, there is a need to develop an efficient algorithm to generate microstructures numerically. The particle packing is initially posed as a nonlinear programming problem and rigorous optimization search algorithms are systematically applied to generate particle systems that are compactly packed, but without particle overlap. Since the packing problem is computationally expensive, the algorithms are systematically evaluated to improve computational efficiency as measured by the number

of particles in the system, as well as the time to generate the microstructure. The evaluated algorithms include the inefficient penalty function methods, best-in-class sequential programming method, matrix-less conjugate gradient method as well as the augmented Lagrangian method. In addition, heuristic algorithms are also evaluated to achieve computationally efficient packing. The evaluated heuristic algorithms are mainly based on the Drop-Fall-Shake method, but modified to more effectively simulate the mixing process in commercial planetary mixers. With the developed procedures, Representative Volume Elements (RVE) with volume fraction as high as 74% were achieved.

After the microstructures were generated, the effective thermal conductivity and effective elastic modulus were estimated using a ‘Random Network Model (RNM)’ that was previously developed. The RNM solves the near-percolation heat conduction problem with hundreds of thousands of particles in minutes compared to hours or days that a full-field simulation requires. The approximations inherent in the RNM are valid if the particulate composite has widely different matrix and particle properties, which is true in the case of thermal greases. In the present thesis, the previously developed RNM was modified to account for the fact that the generated RVEs contain sides with cut particles.

1. INTRODUCTION

Thermal Interface Material, abbreviated as TIM, is used to efficiently dissipate heat from a heat generating component to a heat sink in an electronic package. Most of these interface materials comprise of a base material (e.g. polymer) with highly conducting filler particles (e.g, boron nitride, alumina or sometimes conducting metals such as aluminum or silver) to improve the overall thermal performance of the package. With decreasing size and increasing power and performance of the semiconductor devices, the importance of an efficient thermal management system in the overall product design process is continually increasing. The design of an optimal TIM for desired thermal and mechanical performance is a crucial part of the design of the final product.

1.1 Functionality of TIMs

Heat generated in a semiconductor component needs to be removed efficiently in order to ensure that the operating temperature of the component is within the specified limit. This heat removal process involves transfer of heat from the component surface to a heat sink or heat spreader. For efficient heat transfer, the mating surfaces between the two components need to be in close contact. However, due to limitations in machining processes, the surfaces of the mating components are rough. It is shown that the actual area of contact between the two surfaces is only 1 – 2% of the apparent contact area [1], as shown in Fig. 1.1.

Hence, when two such components are in contact, only the high points are in actual contact and the rest of the area is occupied by air gaps. The presence of these air gaps in the interstitial medium leads to a significant resistance to the heat flow path due to poor conductivity of air. The resistance induced by the air gaps in the

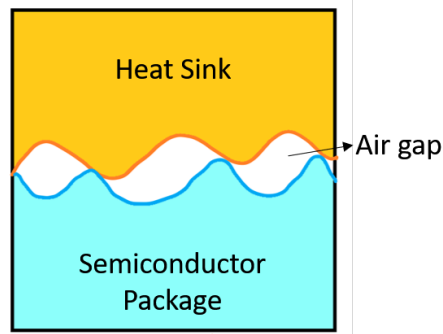


Fig. 1.1.: Presence of interstitial air gaps between contact surfaces

interstitial medium is reduced by using Thermal Interface Materials which conform to the rough and uneven surfaces of the components in contact as shown in Fig. 1.2. A typical heat removal process consists of three modes of heat transfer namely conduction, convection and radiation. However, in the immediate proximity of semiconductor devices, the heat removal is mainly facilitated by conduction through the mating surfaces. TIMs are usually made of highly conducting filler particles dispersed in a polymer base and hence have a higher effective conductivity than air thereby significantly decreasing the resistance across the interface.

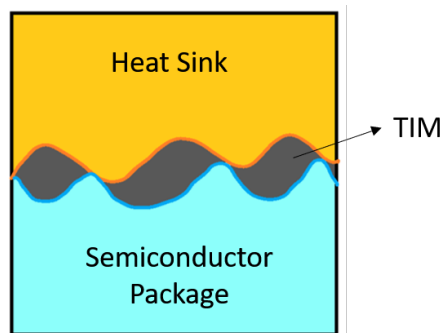


Fig. 1.2.: Conforming TIMs reduce the interstitial air gaps between contact surfaces and decrease thermal resistance

1.2 Thermal Greases and their Modeling

There are various types of TIMs used in the industry based on their application namely thermal greases, thermal gels, thermal pads, thermal adhesive tapes, phase change materials, solders etc. Thermal Greases have the advantages of high bulk conductivity, thin minimal attach pressures and no need for curing [2]. Hence they are used in various fields such as semiconductor packaging, aerospace industry, biomedical industry and automotive industry to name a few [3]. Thermal greases are silicone or hydrocarbon oil based matrices loaded with highly conducting filler particles. Hence the bulk conductivity of the greases increases with increasing volume fractions of fillers in the base matrix. However, as the filler particles have high stiffness, increasing the fillers leads to an increase in the effective stiffness of the matrix and leads to undesired thermal stresses. Hence, there is a need to model the effective thermal conductivity and effective elastic modulus of these particulate composites numerically, so an optimal trade-off between thermal and mechanical response may be achieved.

1.3 Modeling Effective Behavior of TIMs

The majority of research work on TIMs was experimental until late 1990s. Examples of this research include those by Marotta and Fletcher [4], Mirmira et al. [5], Zhou et al. [6]. Thereafter, there have been multiple attempts to estimate the bulk thermal conductivity of TIMs based on classical models, percolation models, finite element models, as well as network models. These modeling approaches are described in detail in Chapter 2.

1.4 Microstructure Generation

In order to estimate the effective properties using the above-mentioned models, numerical simulations need to be performed on microstructures. This in turn requires one to numerically generate microstructures of thermal greases. While factors such as

topology, or particle size distribution, can be used to characterize the microstructure, volume fraction is statistically proven to be a first order descriptor of the microstructure [7]. While early TIMs comprised of filler volume fractions of $\sim 40 - 50\%$, newer thermal greases have filler fractions of $\sim 60 - 80\%$ [3] [8]. Therefore, there is a need to generate microstructures with these ultra-high volume fractions.

There are multiple methods discussed in prior literature to generate microstructures numerically. The problem of packing spheres to generate maximally packed structure dates back to the 17th century. Kepler in 1611 conjectured that the maximum packing density of identical spheres that could be achieved was ≈ 0.74 in a face centered cubic (FCC) arrangement. However, there has been no rigorous mathematical proofs to state the maximum volume fraction of randomly dispersed polydisperse spheres in a closed configuration. In this work, we evaluate various microstructure generation techniques in order to reach the volume fraction of realistic thermal greases. While dynamic methods such as molecular dynamics and discrete element method based simulations [9] can also generate particle-filled microstructures, they are significantly more time consuming since pair-wise particle collision. The static methods discussed in Chapters 4 and 5, on the other hand, are simple to implement and are efficient in terms of computational time.

1.5 Evaluation of Effective Properties

In order to estimate the effective behavior of ultrapacked thermal greases using these newly generated microstructures, the Random Network Model, developed by Kanuparthi et al. [10] was modified in order to incorporate the contributions of the cut particles in the system. In summary, this thesis demonstrates the technique to generate ultrapacked microstructures representing thermal greases and estimate the effective thermal conductivity and elastic modulus of these systems.

2. EVALUATION OF EFFECTIVE PROPERTIES OF PARTICULATE COMPOSITES

Thermal greases are used to expel heat generated from the chip to the heat sink in microelectronic packages as mentioned in Chapter 1. Highly conductive fillers are usually added to a polymer matrix to improve the performance of these thermal greases. The effective thermal conductivity of these particulate TIMs depend on factors such as volume fraction of fillers, morphology of the fillers and distribution of filler materials in the matrix. Significant work has been done in the past to model the effective behavior of such composite materials. The pioneering work in this field was done by Maxwell (1873) and Raleigh (1892). Numerous efforts have since been done to model the effective medium behavior more accurately for a wide range of applications. This chapter provides a review of the classical models as well as the Random Network Model that captures near-percolation behavior of high-contrast particulate composites.

2.1 Classical Models to Evaluate Effective Behavior of Composite Materials

2.1.1 Maxwell's Model

Maxwell, through his 'Treatise on Electricity and Magnetism, 1873', [11] was the pioneer in deriving the effective thermal resistivity of composites. The electric potential (temperature in case of heat conduction) satisfies the Laplace Equation. Maxwell proposed the effect of far-field conditions to have no effect on the near-field region, i.e, the effect of placing a sphere with a radius of a (with thermal conductivity k_f) in an infinitely homogeneous medium (with thermal conductivity k_m) was considered

to have no effect at a distance far away from the sphere, as shown in Fig. 2.1. The governing equations and boundary conditions are described in Eqs. (2.1) - (2.5).

$$\text{Governing equation : } \nabla \cdot q = 0 \quad (2.1)$$

where,

q - heat flux inside the sphere

$$\text{Fourier's Law : } q = -k \cdot \nabla T \quad (2.2)$$

from (2.1) and (2.2),

$$\nabla^2 T = 0 \quad (2.3)$$

Boundary conditions :

$$\begin{aligned} T|_{r=a^-} &= T|_{r=a^+} \\ k_p \frac{\partial T}{\partial r} \Big|_{r=a^-} &= k_m \frac{\partial T}{\partial r} \Big|_{r=a^+} \end{aligned} \quad (2.4)$$

k_p - Thermal conductivity of the filler particle in W/(m-K)

k_m - Thermal conductivity of the matrix in W/(m-K)

Far - field conditions :

$$\frac{\partial T}{\partial r} \Big|_{r=\infty} = \text{constant} \quad (2.5)$$

Solving the governing equation together with the boundary conditions,

$$\begin{aligned} T_\infty &= \left(C_0 R + \frac{C_1}{R^2} \right) \cos \theta \\ \text{where } C_1 &= \frac{k_m - k_p}{2k_m + k_p} R^3 C_0 \end{aligned} \quad (2.6)$$

Maxwell extended this result to a system of a large spheres of radius r containing n smaller spheres of radius a using the principle of superposition. The effective conductivity, k_{eff} was then solved for by applying the boundary conditions and considering the volume fraction, $\phi = \frac{na^3}{R^3}$ as:

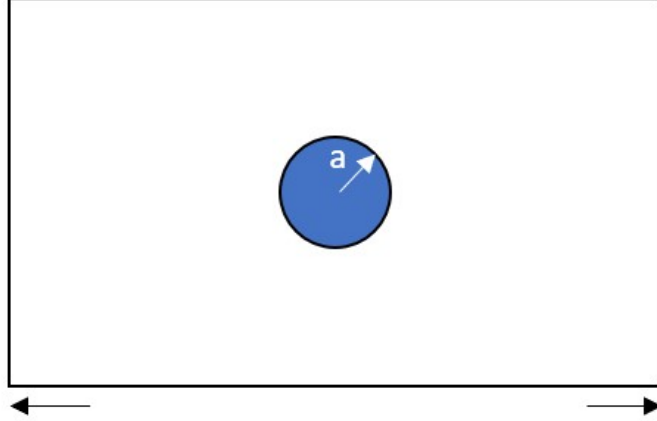


Fig. 2.1.: Particle of radius a in infinite medium

$$k_{eff} = \frac{1 + 2\beta\phi}{1 - \beta\phi} k_p \quad \text{where} \quad \beta = \frac{k_p - k_m}{k_p + 2k_m} \quad (2.7)$$

Eq. (2.7), known as the Maxwell-Garnett equation, gives the effective conductivity of n spherical filler particles in a continuous matrix. This equation however is valid only for “dilute” systems, where inter-particle interactions may be ignored. Numerous models have since been developed that modify and extend this model to evaluate the effective behavior of particulate systems.

2.1.2 Rayleigh Model

Rayleigh [12] considered the effect of filler particles by considering a system of spherical inclusions arranged periodically in a simple cubic arrangement as shown in 2.2. This model accounts for inter-particle interactions by evaluating contributions of every inclusion from its neighbors. The formula for calculating the effective conductivity derived by Rayleigh is:

$$\frac{k_{eff}}{k_m} = \left\{ 1 + \frac{3\phi}{\frac{k_p - 2k_m}{k_p - k_m} - \phi + 1.569 \left(\frac{k_p - k_m}{3k_p - 4k_m} \right) \phi \frac{10}{3} + \dots} \right\} \quad (2.8)$$

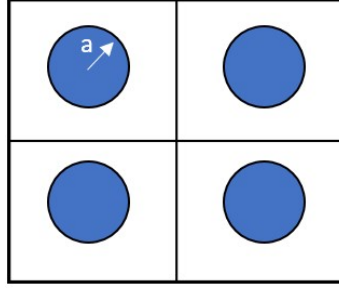


Fig. 2.2.: Regular arrangement of spheres in a simple cube

It can be seen that when the higher order terms are ignored, Eq. (2.8) reduces to Maxwell's formula. Rayleigh also extended this to model cylindrical inclusions placed in parallel in a cubic cell. However, Rayleigh's model only applies for regular arrangement of equi-sized fillers. McKenzie et al.(1978) [13] extended Rayleigh's model to include alternative periodic arrangements such as face-centered cubic and body-centered cubic.

2.1.3 Hasselman-Johnson Model

Hasselman and Johnson [14] model accounts for the influence of interfacial thermal resistance ($\frac{1}{h_c}$) due to the presence of gaps between particles. The temperature continuity equation at the interface is modified to include the effect of the interfacial thermal resistance and hence this model also accounts for the influence of radius of the fillers on the effective conductivity of the composites. The Hasselman-Johnson model which is a modification to the Maxwell and Rayleigh models is described in Eq. (2.9) :

$$\frac{k_{eff}}{k_m} = \frac{\left[2 \left(\frac{k_p}{k_m} - \frac{k_p}{ah_c} - 1 \right) \phi + \frac{k_p}{k_m} + 2 \frac{k_p}{ah_c} + 2 \right]}{\left[\left(1 - \frac{k_p}{k_m} + \frac{k_p}{ah_c} \right) \phi + \frac{k_p}{k_m} + 2 \frac{k_p}{ah_c} + 2 \right]} \quad (2.9)$$

2.1.4 Bruggeman's Asymmetric Model

The Bruggeman's Asymmetric Model (BAM) [15] is a differential effective medium approximation (DEM) method of incremental homogenization. Bruggeman through his DEM method assumed that the composite may be constructed incrementally by introducing infinitesimal changes to already existing medium. The differential form is given by Eq. (2.10)

$$dK = 3K \frac{d\phi' [K_d(1 - \alpha) - K]}{(1 - \phi') [K_d(1 + 2\alpha) + 2K]} \quad (2.10)$$

where $\alpha = \frac{a_k}{a}$ and $a_k = R_{int}k_m$.

α is a dimensionless parameter which depends on the Kaptiza radius, a_k .

BAM allows the modeling of multi-phase components and is accurate for high volume fraction systems. Every and Tzou [16] extended BAM to incorporate interfacial thermal resistance. The equation to calculate the effective conductivity is given by:

$$(1 - \phi)^3 = \frac{k_m}{k_{eff}} \left(\frac{1 + 2\alpha}{1 - \alpha} \right) \left[\frac{k_{eff} - k_p(1 - \alpha)}{k_m - k_p(1 - \alpha)} \right] \left(\frac{3}{1 - \alpha} \right) \quad (2.11)$$

2.2 Percolation Based Models

Network based percolation models aim to numerically simulate percolation theory in composite mediums containing high volume fraction of filler particles. In a system with high volume fraction, percolation theory probabilistically determines a continuous path that connects the particles to form a chain of flow for the heat flux as shown in Fig. 2.3. Devpura et al. [17] showed that the probability of forming these continuous paths is dependent on the volume fraction. On reaching a *percolation*

threshold of volume fraction, the continuous chain is almost certainly formed. It is seen that once such a continuous chain is formed, the heat flow predominantly occurs through these chains as opposed to the heat flow across the matrix materials. This assumption, and hence network-based percolation models are strictly valid only in cases where the ratio of $\frac{k_p}{k_m} \rightarrow \infty$. While this model cannot handle random arrangement and distribution of fillers, Devpura performed simulations on spherical particles, rods and flakes and reported that the systems which had these filler particles along the direction of heat flow were found to have better effective thermal behavior.

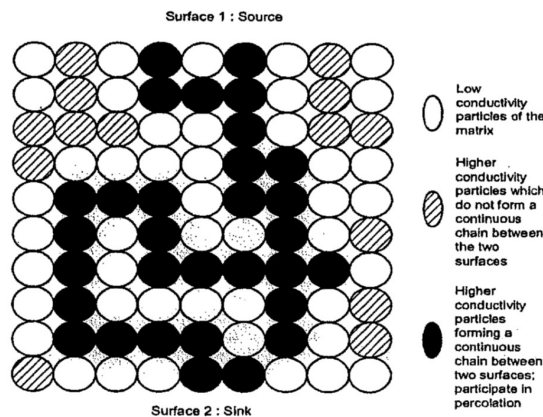


Fig. 2.3.: Percolation: Formation of continuous chain of highly conducting particles (Devpura et al. [17])

2.3 Full-field Meshless Simulations

Natekar et al. [18] and Zhang et al. [19] developed a multi-scale meshless modeling technique termed as Hierarchical Partition of Unity Field Compositions (HPFC) to perform geometry-based meshless analysis where complex geometries are constructed through Boolean operations on simple primitive geometries. The analysis is carried out over the primitives by using NURBS (Non-uniform rational B-spline) based meshless discretization. The temperature and displacement fields are approximated on the primitives and then composed appropriately to obtain solution fields on complex ge-

ometries. These are full-field simulations as they do not make network or lumped approximations in modeling the temperature fields in the system. These models promise greater accuracy, but are computationally very expensive.

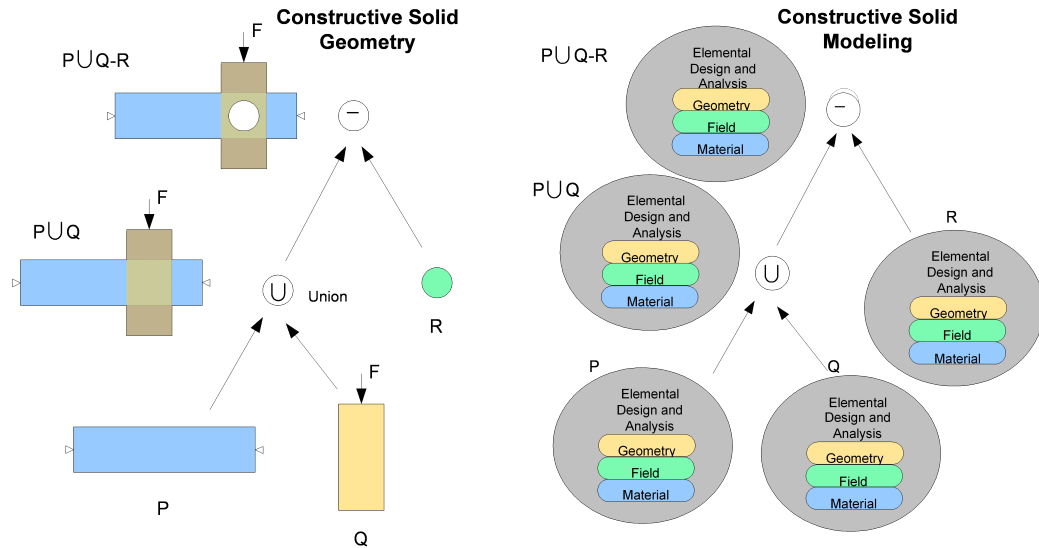


Fig. 2.4.: Constructive modeling strategy that enables hierarchical operations on geometry, analysis fields and materials (source: Zhang et al. [19]).

Kanuparthi [20] carried out full-field simulations of 3D microstructures for high contrast particle filled TIMs using an object-oriented symbolic framework for integrated mesh-less analysis and optimal design called jNURBS. The results of the simulations were shown to be in excellent correlation with experiments of particles with identical volume fraction. In the simulations, large fluxes in the neighborhood of points of contact in particles in near proximity was observed, as shown in Fig. 2.5. Kanuparthi then inferred that energy transfer happens predominantly through these near-contact points (for high contrast systems) and the full-field simulations were accurate because they accurately captured the spatial arrangement of the particles, which in turn allowed the model to capture the near-percolation behavior. The simulations were accurate relative to the experiments even though the simulated microstructures were different from those in the experiments because the statistics of

the gap between particles (matrix exclusion probability) matched that of the particles in the experimental system.

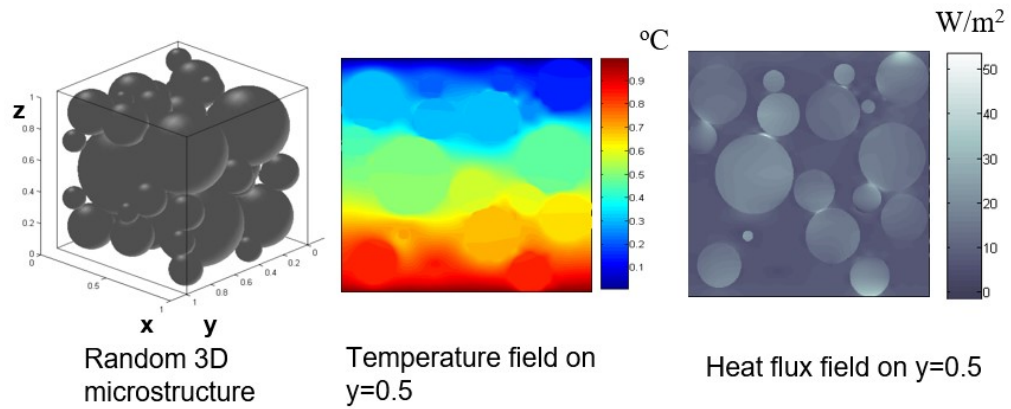


Fig. 2.5.: (a) Temperature and (b) heat flux fields obtained at the midplane of the (c) microstructure ($y = 0.5$) using jNURBS.(source: Kanuparthi et al. [20]).

3. RANDOM NETWORK MODEL

The classical models and percolation models, as explained in Sec. 2.1 and Sec. 2.2, assume a uniform particle size and a regular arrangement of particles. The values predicted using these models become less accurate for systems with volume fraction $> 30\%$. As commercial TIMs have fillers with volume fractions $> 55\%$, an alternative model is required to estimate the effective properties. Kanuparthi et al. [20] recognized that the particle systems mostly exhibit near-percolation behavior that can be captured accurately with full-field simulations provided the matrix exclusion probability in simulated microstructures matched that in the experiment. However, the full-field simulations were computationally very expensive, hence Kanuparthi et al. [10] developed a computationally efficient network model to efficiently capture the near-percolation transport by capturing the pairwise interactions. The model utilizes an analytical estimate of the gap conductance between two spherical particles to estimate the effective conductance of two particles in near percolation configuration. This configuration is then extended into a network considering pair-wise particle interactions. The RNM was validated both against full-field simulations and against experiments. It was shown to be very efficient in predicting the effective thermal conductivity of particulate composites. RNM seeks to replace the system of fillers in a matrix with an equivalent network of resistors as shown in Fig. 3.1. The RNM was extended by Vaitheeswaran et al. [21] to estimate the effective elastic modulus of the particulate composites, thus aiding in designing of thermal greases with optimal thermal and mechanical properties. A brief description of the RNM is provided in this section.

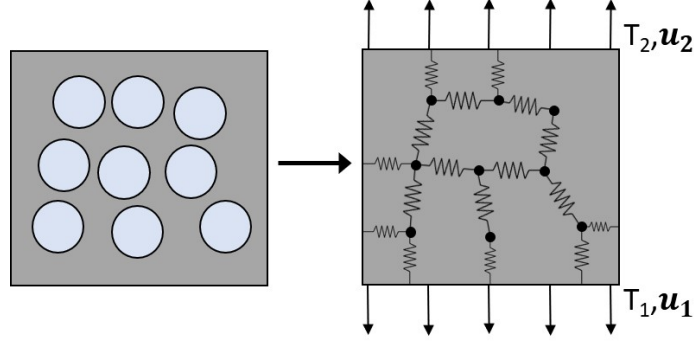


Fig. 3.1.: Network of resistors (source: Kanuparthi [10])

3.1 Development of RNM

Consider the case of one-dimensional heat transfer in a uniform bar of thermal conductivity, k with a cross-sectional area A and length L (conductance $K = \frac{kA}{L}$). The conductance matrix for this is given by:

$$\begin{bmatrix} K & -K \\ -K & K \end{bmatrix} \begin{bmatrix} T_1 \\ T_2 \end{bmatrix} = - \begin{Bmatrix} q_1 \\ q_2 \end{Bmatrix} \quad (3.1)$$

In order to consider a system with many particles in a matrix, Kanuparthi et al. [10] formulated an expression for the local inter-particle conductance matrix from Batchelor's analytical model for gap conductance estimation. Batchelor [22] proposed that the heat flux between spherical fillers is approximately confined to a cylindrical zone of radius R_{12} and gap h_{12} as shown in Fig. 3.2.

The value of conductance due to the fillers and the matrix was derived as shown in Eq. (3.2):

$$K_{gap} = \pi k_m a_{12} \log \left(1 + \frac{R_{12}^2}{a_{12} h_{12}} \right) \quad (3.2)$$

where

K_{gap} — Conductance in the gap between two spherical particles as shown in Fig. 3.2

k_m – Conductivity of the matrix material

h_{12} – Gap between two particles

a_{12} – Mean curvature of radius given by Eq. (3.2)

$$a_{12} = \frac{2R_1R_2}{R_1 + R_2} \quad (3.3)$$

and

$$\begin{aligned} K_1 &= \frac{k_p \pi R_{12}^2}{R_1} \\ K_2 &= \frac{k_p \pi R_{12}^2}{R_2} \end{aligned} \quad (3.4)$$

where K_1 and K_2 are the conductance of particle 1 and 2.

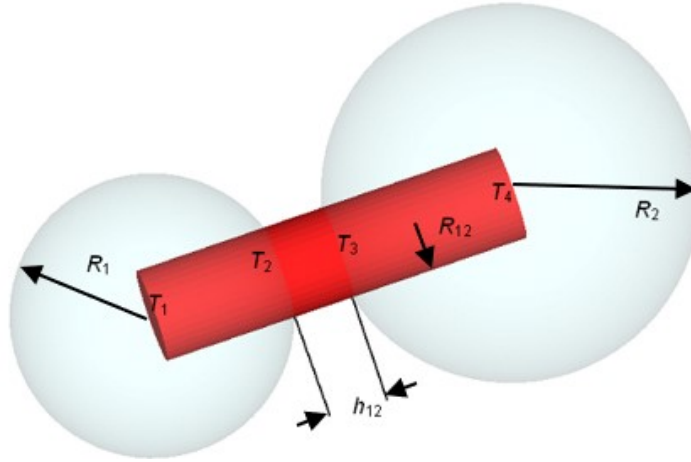


Fig. 3.2.: Cylindrical zone of heat transfer (source: Kanuparthi [10])

The local conductance of inter-particle system can now be written as:

$$\frac{1}{K} = \frac{1}{K_1} + \frac{1}{K_{gap}} + \frac{1}{K_2} \quad (3.5)$$

In a similar manner, instead of Particle 2, the conductance corresponding to interaction with the wall is also estimated (described below and in detail in [10]) Once the local conductance matrices for the inter-particle and the wall interactions are

calculated, the global conductance matrix for the microstructure is assembled. Constant temperature boundary condition is applied on the top and the bottom of the microstructure, while the sides are considered adiabatic. The nodal temperatures is solved for, which gives the value of flux that enters and leaves the microstructure. This is then used to calculate the effective thermal conductivity of the matrix.

Now that an expression for the interaction between particles has been derived, the expression for interaction of a particle with a wall (or edge of the microstructure) needs to be derived. This is done by approximating the wall as a particle with infinite radius.

Two particles are said to be interacting if the gap between two particles is less than a specified threshold. Similarly, the interaction of the particle with a wall is considered if the particle is less than a threshold distance away from the wall.

Dan et al. [23] extended this derivation to modify the cylindrical region to a system with semi-spherical regions connected with a cylindrical zone by as shown in Fig. 3.3. The conductance of the system with the semi-spherical region is as shown in Eq. (3.6).

$$\begin{aligned} \frac{1}{K_1} &= \frac{1}{2\pi R_1 k_p} \log \left(\frac{R_1 + \sqrt{R_1^2 - R^2}}{R_1 - \sqrt{R_1^2 - R^2}} \right) \\ \frac{1}{K_2} &= \frac{1}{2\pi R_2 k_p} \log \left(\frac{R_2 + \sqrt{R_2^2 - R^2}}{R_2 - \sqrt{R_2^2 - R^2}} \right) \end{aligned} \quad (3.6)$$

$$\frac{1}{K_{gap}} = \frac{1}{\pi k_m a_{12} h_{12} \log \left(1 + \frac{R^2}{a_{12} h_{12}} \right)}$$

3.1.1 Validation of Random Network Model

Kanuparthi performed extensive experimental and numerical simulations in order to compare the results of the Random Network Model described in reference [10]. Fifteen samples each of two different systems (alumina fillers in silicone matrix and

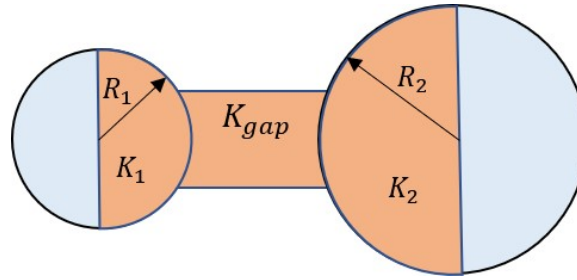


Fig. 3.3.: Semi-spherical zone of heat transfer in the fillers (source: Vaitheeswaran et al. [21])

aluminum fillers in silicone matrix) with 58% filler fractions were prepared. The bulk conductivity of these samples were measured using Laser Flash test methodology as shown in Fig. 3.4.

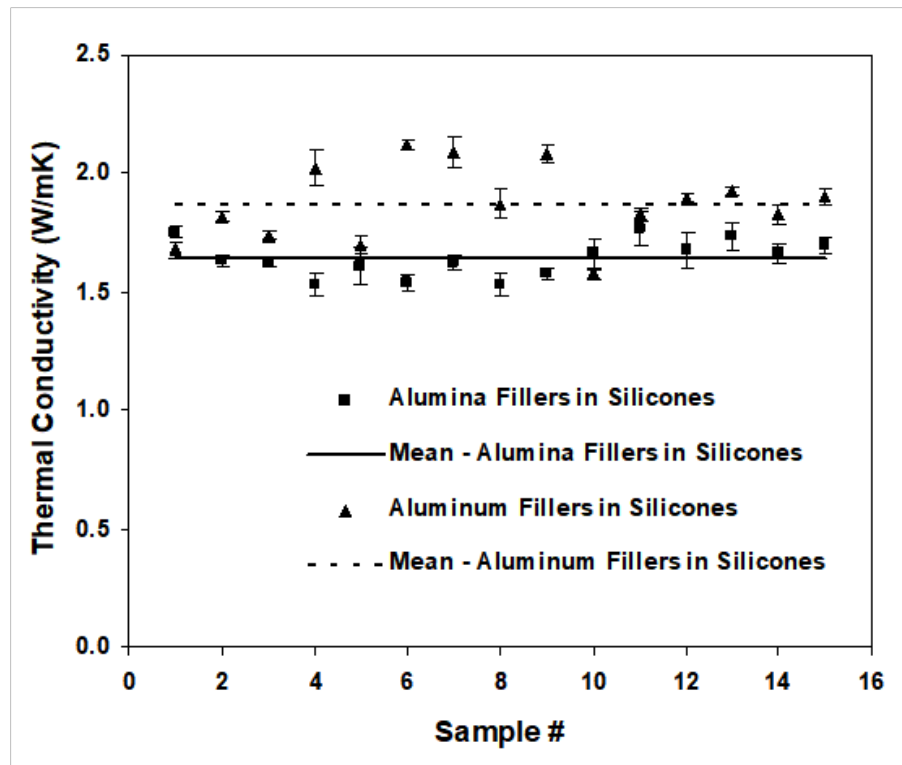


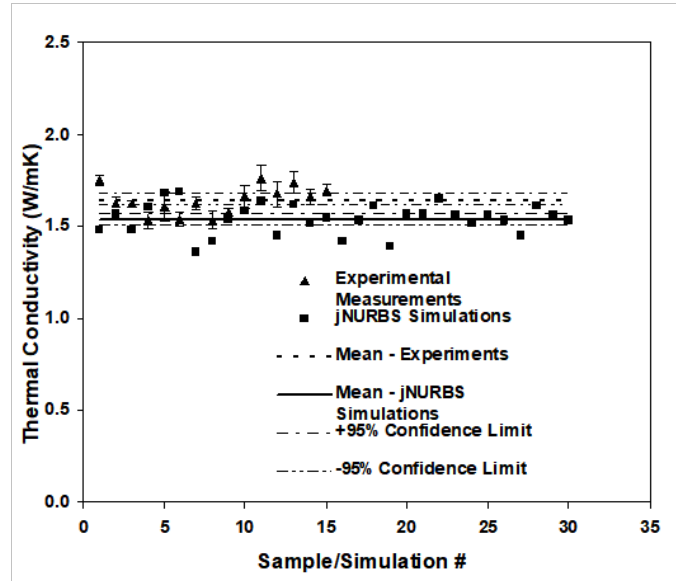
Fig. 3.4.: Experimental effective thermal conductivity of samples (source: Kanuparthi [10])

Full field simulations using jNURBS were then performed using thirty microstructures of the same filler-matrix combination with 58% filler fractions in order to compare the accuracy of these numerical simulations against that of the experimental results as shown in Fig. 3.5. The results of the numerical simulations were found to be in very good agreement with the experimental values and the mean value of the simulations of these microstructures was within 10% of the mean of the experimental values.

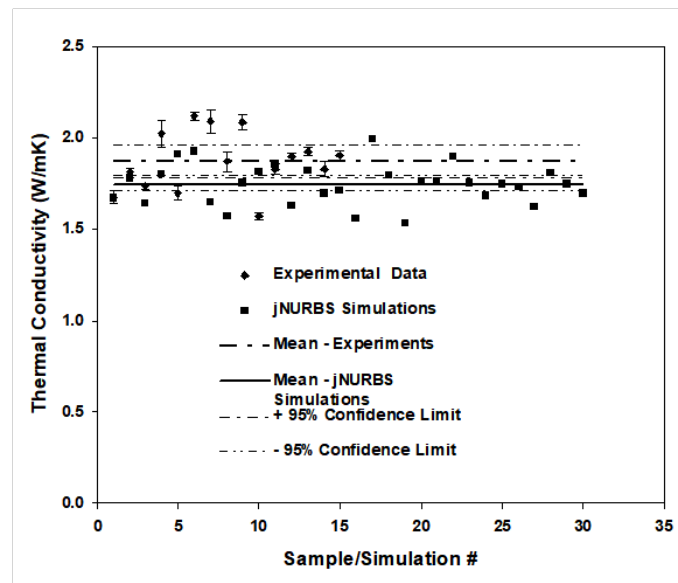
After having validated the results of the full-field simulations, Kanuparthi performed the Random Network Model analysis using twenty microstructures representing the system of Alumina fillers in Silicone matrix at 58% volume fraction. The results of this analysis using the RNM were compared with those of the full-field simulations results (using jNURBS) as shown in Fig. 3.4. The values were found to be in close agreement and within 10% variation as compared to the numerical simulations. Thus, the results of the Random Network model were found to capture the near-percolation physical behavior of the real systems reliably.

3.2 Estimation of Effective Elastic Modulus Using Random Network Model

Highly conductive fillers are embedded in a base matrix in order to increase the overall conductivity of the system. But the filler particles are usually much stiffer than the matrix material leading to undesirable thermal stresses on the brittle silicon device. Hence, in order to estimate the effective modulus, Vaitheeswaran et al. [21] developed formulation analogous to thermal conductance for elastic stiffness of particulate systems. As in the case of heat conduction, the force transfer between particles is assumed to be restricted to a cylindrical zone of interaction as shown in Fig. 3.7. In order to obtain a local stiffness matrix, the gap stiffness was obtained using the procedure followed in Batchelor's derivation mentioned earlier [22]. Thus, Eq. (3.7)



(a)



(b)

Fig. 3.5.: Comparison of numerical simulations with experimental results of (a) alumina fillers in silicone matrix (b) aluminum fillers in silicone matrix (source: Kanuparthi [10])

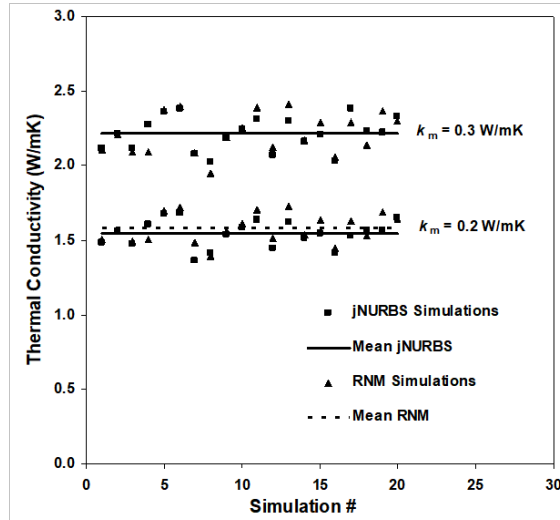


Fig. 3.6.: Comparison of RNM results with Full-field simulations (source: Kanuparthi [10])

estimates the stiffness of the filler particles for the semi-spherical zone shown in Fig. 3.3.

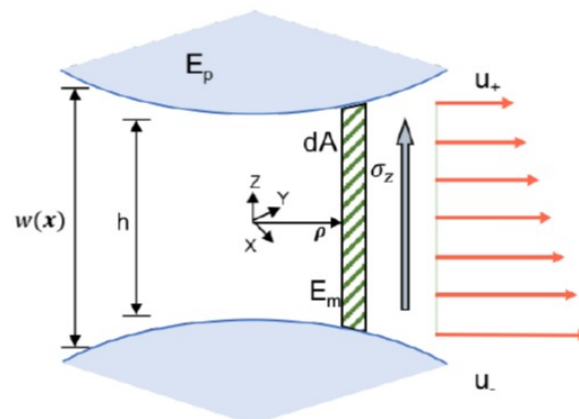


Fig. 3.7.: Force transfer across the matrix layer (source: Vaitheeswaran et al. [21])

$$\frac{1}{E_{12}} = \left\{ \frac{\log \left(\frac{R_1 + \sqrt{R_1^2 - R^2}}{R_1 - \sqrt{R_1^2 - R^2}} \right)}{2\pi R_1 E_p} + \frac{1}{\pi E_m a_{12} h_{12} \log \left(1 + \frac{R^2}{a_{12} h_{12}} \right)} + \frac{\log \left(\frac{R_2 + \sqrt{R_2^2 - R^2}}{R_2 - \sqrt{R_2^2 - R^2}} \right)}{2\pi R_1 E_p} \right\} \quad (3.7)$$

The global stiffness matrix is then assembled as before. The displacement boundary conditions are applied on the top and bottom surfaces while the sides are assumed to be fixed. The nodal displacements are calculated, which gives the force transmitted across the top and bottom surfaces. The effective modulus is then calculated using these values.

3.3 Extension of RNM for Modified Microstructures

The Random Network Model discussed thus far describes the procedure to evaluate the effective properties of random microstructures. The microstructures considered previously comprised of complete spherical fillers in a base matrix. However, typical volumetric subregions of thermal greases have partially cut particles along the edges of the microstructure as depicted in Fig. 3.8. The contribution of these partial particles needs to be evaluated in order to calculate the effective conductivity of these representative volume elements (RVEs) accurately. This section describes the extension to the RNM in order to evaluate the contribution of the partially cut particles in the microstructure.

3.3.1 Derivation of Limits for Inter-particle Conductance

Sec. 3.1 described the motivation and detailed formulation of the Network Model to estimate the effective conductivity of particulate thermal greases. Eq. (3.2) and (3.5) gives the effective conductance of two interacting particles and the interactions

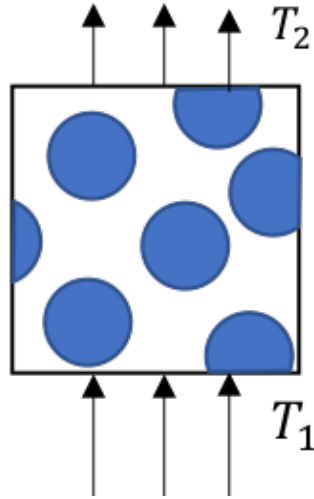


Fig. 3.8.: Network of resistors in the RVE

with walls by considering the radius of the wall to be infinite. Further, it was stated that Dan et al. [23] extended the model to consider a semi-spherical zone of conductance within the interacting particles. A brief derivation of this model is first provided before deriving the extended model for cut particles.

One dimensional heat conduction is assumed across the interface in order to calculate the conductance of the semi-spherical region. The area of the semi-spherical region is obtained by integrating a small strip of length dx along the center of the particle as shown in Fig 3.9 and described in Eq. (3.8).

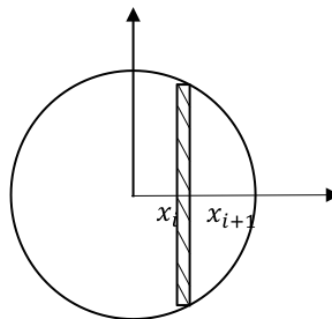


Fig. 3.9.: Integrating a strip of length dx across the x- axis

$$\frac{1}{K_1} = \sum_{i=1}^n \frac{1}{K_i} = \frac{1}{k_p \pi} \sum_{i=1}^n \frac{\Delta x_i}{R_i^2 - x_i^2} = \frac{1}{k_p \pi} \int_0^{\sqrt{R_1^2 - R^2}} \frac{dx}{R_1^2 - x^2}$$

where (3.8)

R_1 – Radius of the first filler particle

R – Radius of the cylindrical zone

Here, the bounds of integration are from the center of the particle to the point where the cylindrical zone of matrix conductance ends as shown in Fig 3.10. The conductance of filler particle is now calculated by integrating Eq. (3.8). The result of the integration is Eq. (3.9)

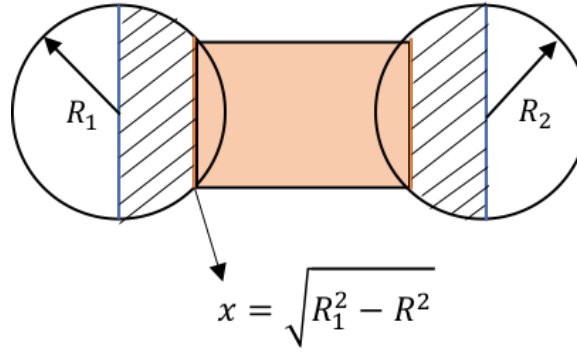


Fig. 3.10.: Integration limits for the semi-spherical zone of conductance

$$\frac{1}{K_1} = \frac{1}{2\pi R_1 k_p} \log \left(\frac{R_1 + \sqrt{R_1^2 - R^2}}{R_1 - \sqrt{R_1^2 - R^2}} \right) \quad (3.9)$$

3.4 Extension of Derivation for Cut Particles Along Edges

In order to consider the effect of cut particles along the edges, a modification is made to the derivation explained in Sec. 3.3.1. In the previous derivation, the limits of the integration start at the center of the particle and end at the point where the cylindrical zone begins as shown in Fig. 3.10. But in order to consider the effect

of particles cut along all edges, the limits of integration vary based on the extent of interaction of the cut particle with the wall as shown in Fig. 3.11.

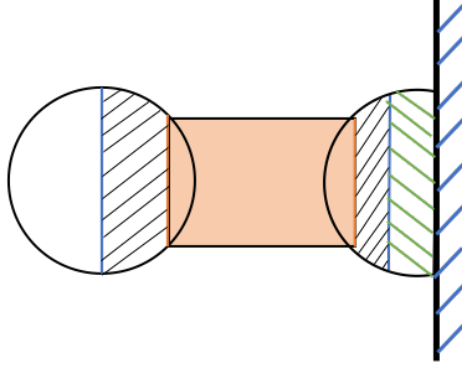


Fig. 3.11.: Semi-spherical model for cut particles

The bounds on the integration in this case needs to be evaluated based on the direction of interaction with the wall as shown in Fig. 3.11. Thus, in case of cut particles, the interaction with all the edges of the RVE needs to be evaluated in order to account for the contribution of conductance from the cut particles (the green shaded region in Fig. 3.11). The new modified integral is described in Eq. (3.10)

$$\begin{aligned} \frac{1}{K_{cut}} &= \frac{1}{k_p \pi} \int_{lb}^{ub} \frac{dx}{R_1^2 - x^2} \\ \frac{1}{K_{cut}} &= \frac{1}{2\pi R_1 k_p} \log \left(\frac{R_1 + ub}{R_1 - ub} \times \frac{R_1 + lb}{R_1 - lb} \right) \end{aligned} \quad (3.10)$$

where

lb = Center of filler particle (x_i)

ub - Distance from the center of the filler to the edge (x_{wall})

$$\frac{1}{K} = \frac{1}{K_1} + \frac{1}{K_{gap}} + \frac{1}{K_2} + \frac{1}{K_{cut}} \quad (3.11)$$

The local conductance matrix for these new systems is now calculated as described by Eq. (3.11). The total flux and force in the RVE is calculated using these new equations for cut particles and assembled into the global conductance and stiffness matrix in order to calculate the effective conductivity and elastic modulus of the

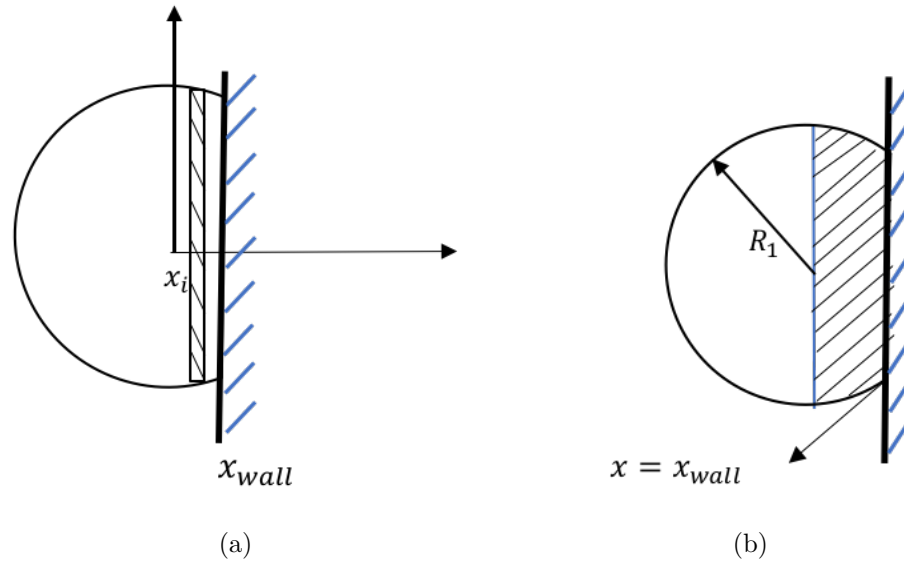


Fig. 3.12.: Modified particle conductance (a) integration of the strip from center of the particle to the edge (b) conductance of the cut particle

thermal grease. Chapter 4 and Chapter 5 describe the various numerical techniques to generate microstructures in order to carry out the RNM simulations. The effective behavior of the simulated systems estimated using the Modified Random Network Model are also discussed in Chapter 5.

4. COMPARATIVE EVALUATION OF ALGORITHMS FOR MICROSTRUCTURE GENERATION

The Random Network Model (RNM), as described in Sec. 3 evaluates the effective thermal and mechanical properties of a composite medium consisting of spherical filler particles in a matrix. In order to use the Random Network Model, a microstructure representing the composite medium (e.g, thermal greases) needs to be numerically generated. A structure in which the microscopic length scale is much larger than the molecular dimensions, but much smaller than the length of the macroscopic sample is called a microstructure [7]. This chapter gives a description of the preliminary algorithms used to generate microstructures.

Microstructures are used as Representative Volume Elements (RVEs) to perform numerical simulations in order to estimate the effective behavior of the particulate systems. In order to calculate the effective properties of thermal greases using Random Network Model as described in Sec. 3, and to validate the results with the classical models, ‘random’ microstructures need to be generated with varying volume fractions. The volume fractions of commercially used thermal greases are often as high as 60 – 80% [3]. Hence, algorithms need to be developed that can generate microstructures with high volume fractions in this range.

The problem of finding the configuration that provides the maximal packing efficiency has long confounded researchers. One of the earliest geometrical explanations was provided by Kepler in 1611. He conjectured that the maximum packing density of identical spheres that could be achieved was $\phi_{max} = \pi/\sqrt{18} \approx 0.74$ by considering a face centered cubic (*fcc*) arrangement. Centuries later, Hales [24] presented a rigorous proof for Kepler’s conjecture, which is still under evaluation. While this provides the maximum limit for regularly packed spheres, the problem of randomly packing spheres in a closed region remains an open problem. The limit of random

close packing (*rcp*), otherwise termed as ‘Maximally Random Jammed (MRJ)’ state by Torquato [25] claims the maximum volume fraction of non-overlapping 3D spheres to be ≈ 0.64 . While the above predictions hold good for infinitely large systems, real systems often contain limited number of particles confined by boundaries. These restrictions lower the value of numerically achievable maximum volume fraction. With this limit as a target, suitable Optimization Techniques and Random Sequential Addition based algorithms have been evaluated in this Chapter in order to generate random microstructures.

4.1 Optimization Techniques to Generate Microstructures

‘Sphere Packing Problems’ refer to the set of mathematical problems that attempt to pack 3-D spheres into containers. Microstructure generation can be posed as a Sphere Packing Problem by formulating it as an optimization problem. The objective of this problem is to minimize the gap between every particle in a container or box, in order to obtain a microstructure with a very high volume fraction. A constraint is applied to ensure no overlap between any pair of particles in the system. This is pictorially represented in Fig. 4.1.

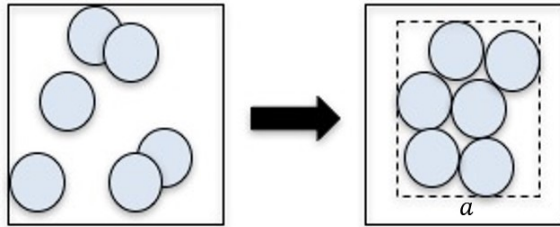


Fig. 4.1.: Optimization technique to pack spheres in a cube

The general formulation of this optimization problem is as shown below:

$$\underset{x}{\text{minimize}} \quad \sum_{i=1}^n \sum_{j=i+1}^n \|x_j - x_i\| \quad (4.1a)$$

$$\text{subject to} \quad \|x_j - x_i\| - [R_j + R_i] \geq 0 \quad \forall i = 1, 2 \dots n \quad \& \quad j = i + 1, i + 2, \dots n \quad (4.1b)$$

$$\text{bounds} \quad x_i - R_i \geq 0 \quad \& \quad x_i + R_i \leq a \quad (4.1c)$$

where,

x_i – position vector of the i^{th} particle of the form $\langle x, y, z \rangle$

n – number of particles in the microstructure

R_i – Radius of the i^{th} particle

a – dimension of the outer box

As seen in Eq. (4.1), this formulation is a nonlinear constrained optimization problem. As both the objective function and constraints are nonlinear, the complexity of the problem increases with the number of particles. For n particles, the number of constraints is of the order n^2 as shown in Table 4.1. Hence, the posing of constraints and their evaluation is an important contributing factor to the solution of the optimization problem. Accordingly, different algorithms that are commonly used to solve the nonlinear optimization problem were evaluated, to arrive at the maximum volume fraction. Sub-chapters 4.1.1 - 4.1.4 describe the methodology and results of the different algorithms.

4.1.1 Exterior Penalty Method

Penalty Methods are one of the simplest algorithms belonging to the group of sequential unconstrained minimization techniques (SUMT) used to solve constrained optimization problems [26]. In the SUMT techniques, the constrained minimization problems are converted into a sequence of unconstrained minimization problems that are easier to solve with readily available unconstrained solvers. The general approach

Table 4.1.: Design variables and constraints

# of Particles	# of Design Variables	# of Constraints
2	6	1
50	150	1225
1000	3000	499500
10000	30000	$\sim 5 \times 10^7$

is to minimize the objective function as an unconstrained function by providing a penalty for every violation of a constraint. The problem might turn out to be numerically ill-conditioned owing to the “penalty” imposition. In order to avoid this, the penalty is moderately imposed initially, and increased sequentially to drive the solution towards the constrained minimum. Thus, the procedure requires solution to a sequence of unconstrained minimization problems each starting with the solution to the previous unconstrained problem until eventually the constrained minimum is reached.

General form of optimization problem is written as:

$$\text{minimize} \quad f(x) \quad (4.2a)$$

$$\text{subject to:} \quad g_j(x) \leq 0 \quad j = 1, 2, \dots, m \quad (4.2b)$$

$$h_k(x) = 0 \quad k = 1, 2 \dots l \quad (4.2c)$$

Exterior Penalty Method is one of the many SUMT algorithms used to solve constrained minimization problems. In this method, an initial guess for the design variable is chosen and if the solution lies in the infeasible region, a penalty is added to the objective function. Thus, the method generally starts with the variables in the infeasible region and subsequent addition of penalty leads to the optimum solution which typically lies on the constraint boundaries. The general form of an optimization problem as shown in Eq. ((4.2)) is now rewritten with a new function called the *pseudo*

objective function is formulated which comprises of both the objective function and the penalty, which is described in Eq. (4.3).

The pseudo objective function, Φ is now written as:

$$\begin{aligned}
 \text{minimize} \quad & \Phi(x) = f(x) + r_p \Psi(x) \\
 \text{where} \quad & \Psi(x) = \sum_{j=1}^m [\max(0, g_j(x))^2] + \sum_{k=1}^l [h_k(x)]^2 \\
 & \Psi - \text{Penalty Function} \\
 & r_p - \text{Penalty Parameter}
 \end{aligned} \tag{4.3}$$

The formulation stated in Eq. (4.3) is used in our problem to generate the microstructures with maximum volume fraction as described in Eq. (4.4). This formulation stands as a template for all the subsequent algorithms described in Sec. 4.1.

The exterior penalty method was implemented in MATLAB for a system with monodisperse particles using the formulation stated in Eq. (4.4). In order to ensure that all the constraints are satisfied, it was observed that the quadratic penalty parameter needs to be very high of the order of 10^8 for a system with 50 particles. With increasing number of particles, the value of penalty parameter needs to be even greater making the problem ill-conditioned. Hence the maximum volume fraction reached using the Exterior Penalty Method was 40% with a system of 50 particles as shown in Fig. 4.2.

$$\begin{aligned}
 \text{minimize} \quad & \Phi(x) = f(x) + r_p \Psi(x) \\
 \text{where} \quad & f(x) = \sum_{i=1}^n \sum_{j=i+1}^n \|x_j - x_i\| \\
 & \Psi(x) = \sum_{l=1}^m [\max(0, g_l(x))^2] \\
 & g_l(x) = [R_j + R_i] - \|x_j - x_i\| \\
 \forall i = 1, 2, \dots, n \quad & \text{and} \quad j = i + 1, i + 2, \dots, n \\
 \text{bounds :} \quad & x_i - R_i \geq 0 \quad \& \quad x_i + R_i \leq a
 \end{aligned} \tag{4.4}$$

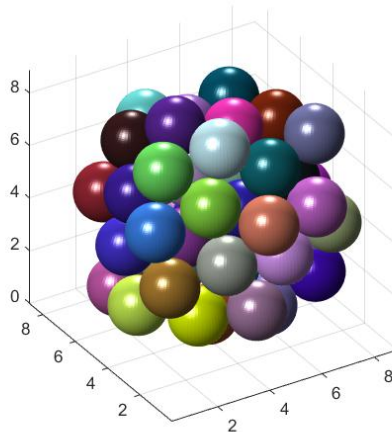


Fig. 4.2.: Microstructure generated with exterior penalty method

4.1.2 Sequential Quadratic Programming Algorithm

The Sequential Quadratic Programming method is commonly considered as one of the most efficient methods for solving nonlinear constrained optimization problems. This method involves iterative generation of solutions for a quadratic subproblem until the solution to the nonlinearly constrained problem is reached. It is a generalization of the quasi-Newton method for constrained minimization as it seeks to find the descent direction, p by minimizing a quadratic subproblem of the form described in Eq. (4.5).

$$\begin{aligned}
 &\text{minimize} && q_k = \nabla f(x)^T p + \frac{1}{2} p^T H p \\
 &\text{subject to:} && \nabla g_i(x) = -g_i \quad i \in I_A \\
 &&& \nabla h_k(x) = -h_k \quad k = 1, 2, \dots, l
 \end{aligned} \tag{4.5}$$

where, I_A is the current estimate of active inequality constraints and $H = \nabla^2 L(x, \mu_i, \lambda_i)$ with

$$L(x, \mu_k, \lambda_i) = f(x) + \sum_{i=1}^m \lambda_i g_i(x) + \sum_{k=1}^l \mu_k h_k(x) \tag{4.6}$$

H is the Hessian matrix of the Lagrangian function L defined in Eq. (4.6). However, in practical implementations, a positive definite, symmetric approximate is made to the

Hessian matrix. BFGS method [27] is one of the most commonly used rank-2 quasi-Newton methods for updating the Hessian approximation. A line-search procedure is performed to calculate the step length in the descent direction of the merit function. The design variable is updated after the resulting step.

In the present study, the SQP method was implemented using the MATLAB Optimization toolbox. It was observed that the maximum volume fraction that could be reached using the SQP algorithm was $\sim 50\%$ for a system of 100 particles as shown in Fig. 4.3. While the SQP algorithm is efficient in terms of number of iterations required for arriving at the solution, the need to estimate and store the Hessian matrix limits the number of design variables that it can handle. Since in our case where there are large number of design variables and constraints, this algorithm becomes very memory intensive. Thus SQP method (implemented in MATLAB) is impractical for systems with a large number of particles. In order to overcome this problem, the "matrix-less" Conjugate Gradient Method was next evaluated as described in Sec. 4.1.3.

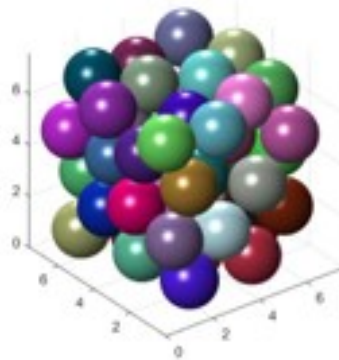


Fig. 4.3.: Microstructure generated with sequential quadratic programming method

4.1.3 Conjugate Gradient Method

Conjugate Gradient Method is one of the many descent or gradient based algorithms used to solve unconstrained nonlinear optimization problems. As with the previously described algorithms, starting from an initial guess, the iterations progress until the convergence criterion is met. The Conjugate Gradient Method uses the concept of “conjugate directions” to arrive at the optimum point in n iterations (for quadratic functions) as opposed to ∞ iterations in Steepest Descent Method. n here refers to the dimension of the problem. The algorithm is briefly described below.

We begin with a brief description of the concept of H-conjugacy.

1. Two directions p_i and p_j are said to be H-conjugate if $p_i^T H p_j = 0 \quad \forall i \neq j$
2. All H-conjugate directions are linearly independent. Hence, a vector \underline{x} can be expressed as $\underline{x} = \beta_1 p_1 + \dots + \beta_n p_n$

The Conjugate gradient method is an iterative method for solving a linear system of equations of the form:

$$Ax = b$$

by solving an equivalent minimization problem of the form:

$$\text{minimize } \phi(x) = \frac{1}{2} x^T A x - b \tag{4.7}$$

where A is symmetric and positive definite. Thus, it is also a technique to minimize convex quadratic functions. The minimization procedure includes an exact line search along a search direction that is a linear combination of the steepest descent direction at the current iterate and the previous search direction. In this method, the property of H-conjugacy facilitates the calculation of new search direction with the help of the residual r and the previous search direction, p . As the search direction vectors are H-conjugate, they are linearly independent with the previous search directions, thus eliminating the need for storing all previous search directions. The various steps involved in the algorithm are described in Algorithm 1. [28].

Algorithm 1 Conjugate Gradient Algorithm

 $r_0 \leftarrow Ax_0 - b, p_0 \leftarrow -r_0, k \leftarrow 0$ **while** $r_k \neq 0$ **do** $x_{k+1} \leftarrow x_k + \alpha_k p_k$ $r_{k+1} \leftarrow r_k + \alpha_k A p_k$ $\beta^{k+1} = \frac{r_{k+1}^T r_{k+1}}{r_k^T r_k}$ $p_{k+1} = -r_{k+1} + \beta_{k+1} p_k$ $k \leftarrow k + 1$ **end while**

Fletcher and Reeves [29] extended the Conjugate Gradient method to solve nonlinear functions by modifying the residual r to be the gradient of the nonlinear function (ϕ from Eq. (4.4) for our case) and performing a line search by minimizing the function along p_k to find the optimum step length, α^* .

The Conjugate Gradient algorithm described above was implemented in FORTRAN programming language using an open-source numerical package called ‘CG+’ [30]. The number of particles in the system was initially increased to 1000 as the algorithm was implemented in a stand-alone FORTRAN code as opposed to being solved within the MATLAB environment with its memory limitations. The maximum volume fraction for this system was $\sim 32\%$ and took ~ 17 hours to complete. In order to increase the efficiency of the algorithm and to decrease the computational time, a nearest neighbor detection method termed *Cells* was implemented. A detailed description of this method is provided in Sec. 4.2.1, but the idea was to sub-divide the domain into cells and to label the particles with the cells to which they belonged. This in turn eliminates the need to do a pair-wise nearest neighbor check for all the particles, as only particles within any given cell need to be checked. By implementing this method, a microstructure with 10000 particles and a maximum volume fraction of $\sim 41\%$ was generated in just 20 minutes. The Conjugate Gradient method is well suited for large optimization problems as it only requires the evaluation of the objective function and its gradient, without the need for tedious matrix operations necessary for the SQP algorithm (Sec. 4.1.2). On the other hand, as the objective function and constraints are nonlinear, the Conjugate Gradient method in turn requires the iterative imposition of constraint penalty resulting in a relatively inefficient solution to the constrained optimization problem.

4.1.4 Augmented Lagrangian Method

The Augmented Lagrangian Method (ALM) also called as the Method of multipliers, is a modification to the quadratic penalty methods described in Section 4.1.2. The general form of Lagrangian function is shown in Eq. (4.8).

$$L(x, \mu_k, \lambda_i) = f(x) + \sum_{i=1}^m \lambda_i g_i(x) + \sum_{k=1}^l \mu_k h_k(x) \quad (4.8)$$

The use of Lagrange multipliers, λ_i and μ_k ensure the necessary conditions for optimality, also called the Karush-Kuhn-Tucker(KKT) conditions. However, the necessary conditions do not ensure that the stationary points are minima of the function. In order to ensure that the solution is the minimum of original function, second order conditions need to be satisfied. In order to satisfy the second order conditions, a quadratic penalty term is augmented to the Lagrangian function such that the Hessian of the Lagrange is positive definite, and hence the name of the algorithm.

In order to augment the Lagrangian for inequality constraint problems, slack variables are added to convert the formulation to equality constraints. However, the Fletcher's substitution as shown in Eq. (4.9) eliminates the need for slack variables. The Augmented Lagrangian formulation, $L(x, \lambda, r_p)$ is shown in Eq. (4.9).

$$L(x, \lambda, r_p) = f(x) + \sum_{j=1}^m [\lambda_j \psi_j + r_p \psi_j^2] + \sum_{k=1}^l [\lambda_{k+m} h_k + r_p h_k^2] \quad (4.9)$$

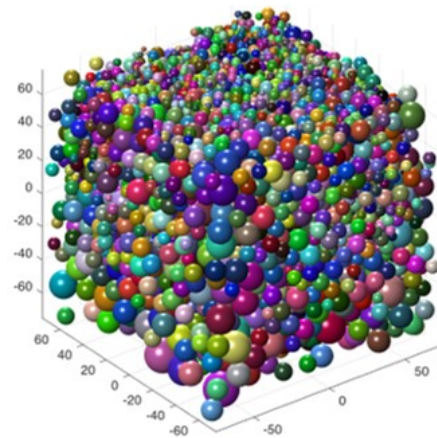
where $\psi_j = \max[g_j, \frac{-\lambda_j}{2r_p}]$

The Augmented Lagrangian function uses the pseudo objective function which has the Lagrange multipliers in addition to the penalty parameters. The solution of the function can be arrived at if the Lagrange multipliers are known. But in practice, the values of λ_i^* is often not known beforehand; the process of solving for exact solution of λ_i^* increases the number of design variables significantly. Hence, most numerical implementations start with initial guess of λ_i and update the value of λ_i along with the penalty parameter in each iteration.

By augmenting the Lagrangian with the quadratic penalty parameters, the number of iterations and the order of penalty imposition significantly decreases. Hence this method leads to well posed formulation of our optimization problem. The Augmented Lagrangian Method was implemented in FORTRAN using an open source numerical software called ALGENCAN [31,32]. The formulation was suited for packing monodisperse spheres in a spherical container. A maximum volume fraction of $\sim 60\%$ was achieved for a monodisperse system in a spherical configuration as shown in Fig. 4.4(a). However, when the formulation was modified to pack monodisperse spheres in a cubic container, the volume fraction decreased to 56%. In order to increase the computational efficiency of the algorithm, Cells method was adopted and the formulation was modified to handle polydisperse (lognormal distributions) spheres. In conclusion, a microstructure was generated with a system of 10000 log-normally distributed spheres with a maximum volume fraction of 60% as shown in Fig. 4.4(b).



(a)



(b)

Fig. 4.4.: Microstructure generated with ALM (a) in a spherical container (b) in a cubic container

4.1.5 Summary of Optimization Techniques

The Optimization Problem of packing three-dimensional spheres efficiently in a cube was implemented using four different algorithms as described in Sec 4.1.1 - 4.1.4. The programming environment of these algorithms was changed from MATLAB to FORTRAN in order to efficiently handle the large number of optimization variables. Starting with a monodisperse system of 50 particles, the size of the problem was increased to handle ~ 10000 particles with a lognormal distribution of particle sizes that was solved within reasonable computation time of 3 – 4 hours on a desktop personal computer (3.6 GHz Intel Core 2 Duo Processor with a memory of 4 GB). Accordingly, the maximum volume fraction was increased from 40% to 60% as summarized in Table 4.2.

Table 4.2.: Summary of optimization techniques

Algorithms Used	# of Particles	Run Time	Volume Fraction Achieved
Exterior Penalty Method	50	40 mins	40%
SQP	100	60 mins	50%
Conjugate Gradient	1000	1020 mins	32%
Conjugate Gradient with Cells	1000	20 mins	43%
Augmented Lagrangian Method	1000	110 mins	55%
Augmented Lagrangian with Cells	100,000	100 mins	60 % (Log-normal)

4.2 Heuristic Algorithm: Drop-Fall-Shake

Having investigated the efficiency of various nonlinear optimization algorithms in Sec. 4.1, we now move on to evaluate heuristic algorithms that sequentially drop particles into a container to maximally pack the container. One of the simple static methods to generate a random microstructure is to place the particles randomly in the matrix. This is done by sorting the size of particles and then by randomly placing the non-overlapping particles inside the container. A random position is generated for every particle; an overlap check is done to ensure there is no overlap between particles. If an overlap is detected, this position is discarded and a new random position is generated until there is no overlap. If this process exceeds a limit on the number of random positions tested, the code is said to have failed. While this method is easy to implement, it only appears to reach volume fractions of up to 35% for three-dimensional microstructures with 50 particles and is very inefficient in system containing large number of particles.

The Drop-Fall-Shake (DFS) method, developed by Smith and Midha [33], described in this section, generates three-dimensional microstructures of required volume fraction by simulating the physical process of dropping and shaking a container with particles in order to maximally pack all the particles. The outline of the method is described below and illustrated in Fig. 4.5.

1. Insert particles into a long container with a low initial volume fraction by randomly placing particles ensuring no overlap between any pair.
2. Sort the particles according to their positions along the z axis and drop particles sequentially to the lower interface of the container. In every step, described by a step length, a random direction is assigned to the particle, ensuring drop in the $-z$ direction.
3. The new position is checked for overlap with other particles; if an overlap is detected, and if a limit on the number of generations of new positions is reached, then the step length is further reduced.

4. If the step length is smaller than a specified value, the particle is assumed to have reached its lowest position.
5. The steps 3 and 4 are repeated for all the particles sequentially.
6. The particles are then given a random shake towards the bottom, albeit with a slight possibility of moving up.
7. Once the required volume fraction is reached, the particles are shaken with an equal probability to move in all directions. This results in random and uniformly distributed microstructure.

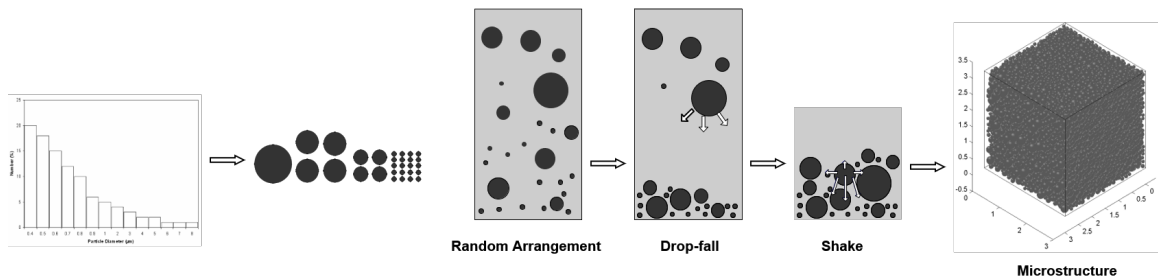


Fig. 4.5.: Schematic representation of Drop-Fall-Shake method.(Source: Zhang. X et al. [19] Smith, LN and Midha, PS [33])

In the DFS procedure, the order of computation for detecting overlaps between n particles is $O(n^2)$. With increasing number of particles, this calculation becomes very time consuming. Hence, a method to detect overlap only between neighboring particles, named *Cells* is used (mentioned in Sec. 4.1.3 and 4.1.4). With the addition of cells, the overall computation time decreases to $O(n)$ and makes DFS quite efficient.

4.2.1 Description of the Cells Method:

The region inside the container is divided into a regular set of smaller cells that maintain a list of particles that are either completely or partially in the cell. Every particle is associated with a cell-list that contains all the cells in which this particle

belongs. Every time a new random position is generated for a particle, the overlap detection is only done between this particle and all particles that are linked to the cell in which it now belongs. This procedure is illustrated in Fig. 4.6.

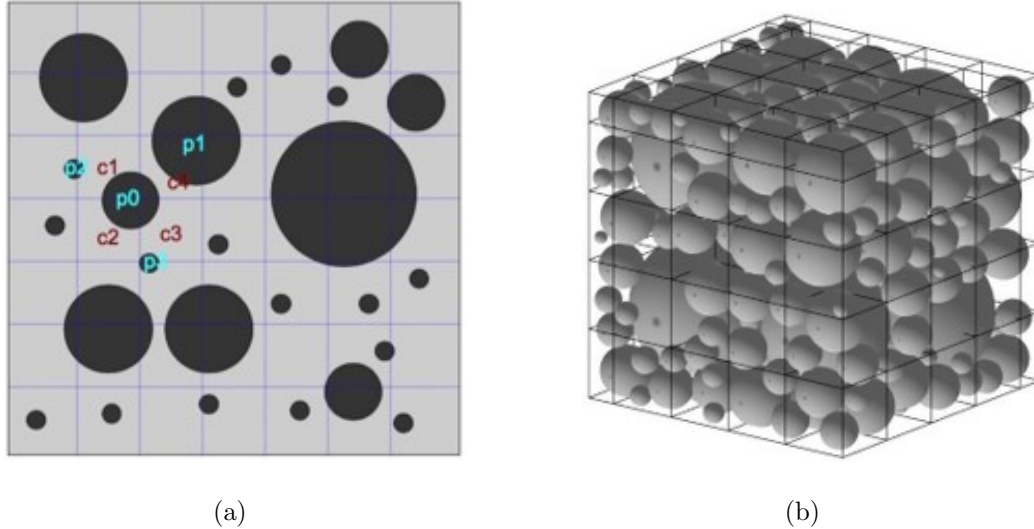


Fig. 4.6.: Cells method to detect overlap only between neighboring particles. (a) cell 1 stores particles p0 and p2 (b) subdivision of 3D microstructures into cells

The cells procedure was used to generate microstructures that were analyzed for effective properties by Kanuparthi [20] and Vaitheeswaran [21]. The maximum volume fraction achieved using Drop-Fall-Shake was 60%.

4.3 Summary of Comparative Algorithm Evaluations

The Sections 4.1 and 4.2 describe the various algorithms and techniques used to generate microstructures with high volume fraction. While the maximum volume fraction of 60% achieved using Optimization Techniques and Drop-Fall-Shake with polydisperse distribution of particles is higher than the reported volume fractions of microstructures using static methods, the need to generate microstructures with very high volume fraction to simulate realistic TIM systems with filler volume fractions

of upto 80% still remains a challenge. The Chapter 5 describes modifications to the DFS algorithm to generate *Ultrapacked Microstructures*.

5. DEVELOPMENT OF ALGORITHMS FOR GENERATING ULTRAPACKED MICROSTRUCTURES

In Chapter 4, after extensive evaluation, it was observed that both the mathematically formulated optimization techniques and sequential random packing using Drop-Fall-Shake could only generate microstructures with volume fractions of $\sim 60\%$. However, the TIMs used in the industry have been found to have filler volume fractions of $\sim 70-80\%$. This chapter describes modifications to the Drop-Fall-Shake algorithm to achieve *ultrapacked microstructures*. The generated microstructures are then analyzed to estimate the effective conductivity as well as modulus using the earlier described random network model.

The commercially produced TIMs use a planetary mixer as shown in Fig. 5.1 to mix particles into the matrix. The dynamic mixing process using rotating double impellers to ensure even mixing and in turn maximal packing of fillers in the matrix material. While the Drop-Fall-Shake algorithm described in Sec. 4.2 incorporates a shake procedure to ensure a random microstructure, the drop procedure attempts to pack particles in the $-z$ direction and does not capture emulate the mixing of particles in a planetary mixer. Therefore, attempt is made to modify DFS algorithm to emulate the mixing process in this chapter.

5.1 Drop-Fall-Mix

The numerical simulations of flow of particles and fluid in a planetary mixer with impellers is complex and challenging [35]. It would require modeling of the relative motion of the fillers with respect to the matrix material. Since the process is dynamic with non-Newtonian flow of the matrix, simulations would entail grid regeneration at every time step. Instead, if one tries to capture a snap shot in time of the mixing,



Fig. 5.1.: Ross Planetary Mixer (source: [34])

the process may appear to involve flow of the particles through the side walls of the container (which represents a control volume) and re-inserting them at the center of the container from the top.

The Drop-Fall-Mix algorithm aims to simulate this flow out of the container through the side walls and re-insertion at the center of the container. This is done by modifying the Drop-Fall-Shake procedure. The steps involved in this algorithm are described below and illustrated in Fig. 5.2.

1. The steps 1–5 from the Drop-Fall-Shake algorithm are performed just as before.
2. The microstructure is divided into four equal blocks along the x direction. The particles (completely and partially) belonging to the outer two blocks close to the edges of the container are removed and their radii are stored separately.
3. The particles remaining in the original microstructure, in the central blocks are now pushed towards the wall on both sides.
4. The removed particles are inserted back into the microstructure by extending the central blocks along the z direction and by generating random non-overlapping locations for particles within these extended blocks.
5. The steps 2 – 7 of the Drop-Fall-Shake procedure are repeated again in order to obtain a random microstructure.

6. The steps 2 – 5 are repeated either until a desired volume fraction or until a limit on the iterations is reached.

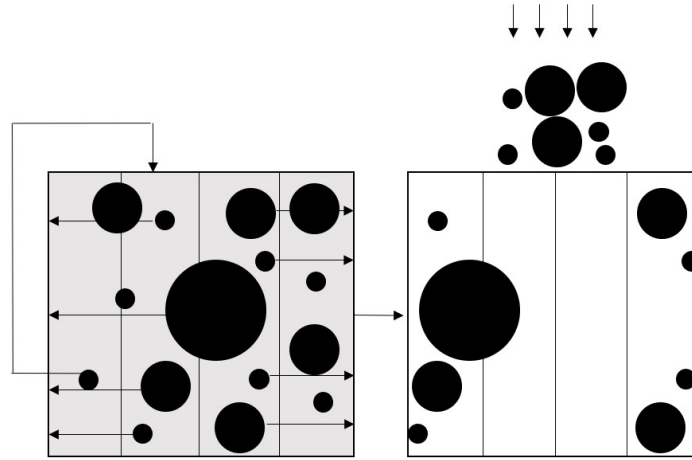


Fig. 5.2.: Schematic representation of Drop-Fall-Mix procedure

This algorithm was evaluated with varying number of particles and sizes of spherical particles with a lognormal distribution. While this algorithm was efficient with less than a thousand particles, the efficiency of the algorithm was limited by the efficiency of the Drop procedure of the Drop-Fall-Shake algorithm for systems with more than 1000 particles. A representative microstructure generated using the Drop-Fall-Mix Procedure is shown in Fig. 5.3. The maximum volume fraction generated by Drop-Fall-Mix algorithm for a system with 10,000 particles was found to be again 60% - not significantly different from that of Drop-Fall-Shake algorithm.

5.2 Modified-Drop-Fall-Shake

The Drop-Fall-Mix algorithm simulates the dynamic process of the planetary mixers by removing the particles in blocks adjoining the side walls of the container and dropping them back in the blocks at the center. But the results of the algorithm were found to be limited by the efficiency of the Drop step. This indicates that in order to maximally pack the particles as in the case of planetary mixers, the algorithm needs

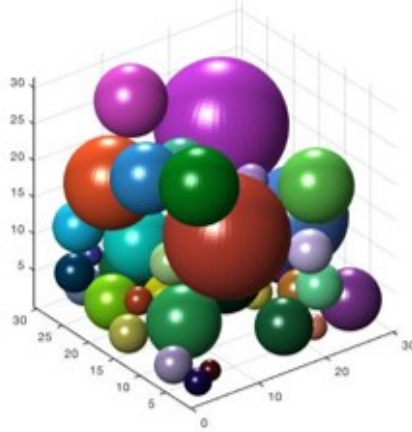


Fig. 5.3.: Microstructure generated with Drop-Fall-Mix method

to be effective in allowing the particles to look for gaps efficiently. This can be facilitated by allowing the particles to move more rapidly along the x and y directions. In the Drop-Fall-Shake procedure, the particle is given a random position by allowing it to move along the x, y and $-z$ directions with equal probability. However, with increasing volume fractions, the gap between particles reduces and, therefore, the probability of efficiently finding the gap reduces. Hence, the algorithm tries to generate a new feasible direction along the $-z$ direction for a certain allowable number of iterations and then moves on to the next particle.

In order to simulate the mixing procedure, a modification is made on the Drop-Fall-Shake procedure. In *Step 2* of Drop-Fall-Shake, instead of allowing the particle to move along x, y and $-z$ directions with equal probabilities, the particles are allowed to move with higher probability along the x and y directions as shown in Fig. 5.4. The slower drop in turn allows for the smaller particles to efficiently move around the larger ones in the x and y directions, allowing them to occupy the gaps in the microstructure efficiently. This modification to Drop-Fall-Shake is termed as the Modified Drop-Fall-Shake Algorithm (MDFS). This new algorithm was able to generate microstructures with ultra-high volume fractions of $\sim 68\%$ with a system of 2×10^5 particles as shown in Fig. 5.5.

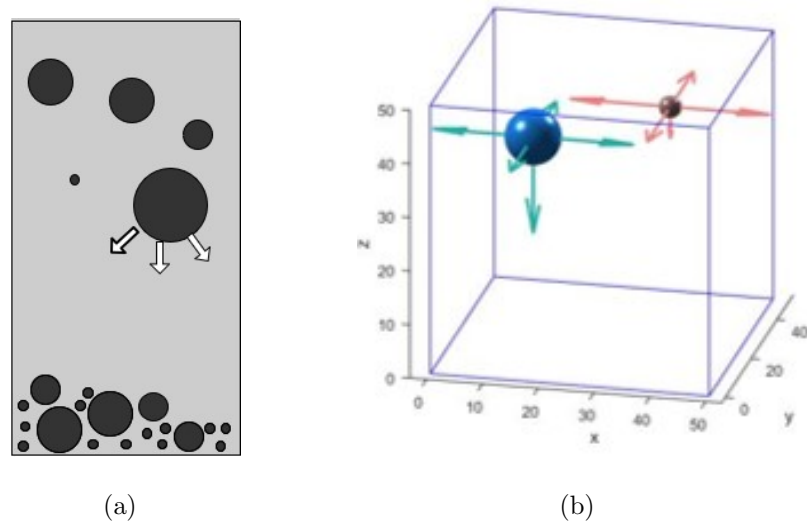


Fig. 5.4.: Modified Drop-Fall-Shake method (a) original Drop-Fall-Shake method (b)modification to allow higher probability to move along x and y directions

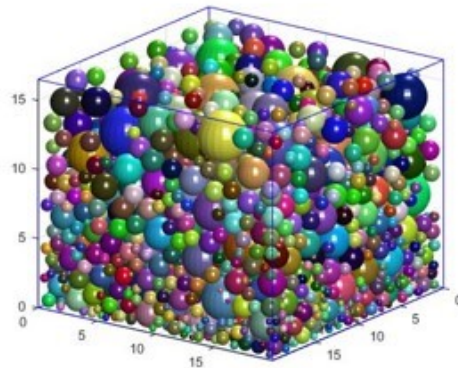


Fig. 5.5.: Microstructure generated using the modified Drop-Fall-Shake method

5.3 Modified-Drop-Fall-Shake with RVE

While the MDFS method can generate microstructures with volume fraction of 68%, there exist regions within the container where the packing is even more efficient as shown in Fig. 5.6. These regions are denoted as representative volume elements (RVE) in the present section. The computation of the actual volume fraction of the

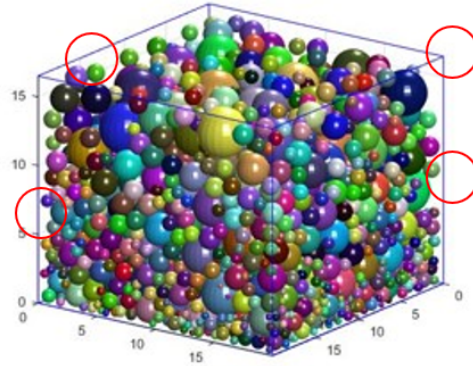


Fig. 5.6.: Presence of gaps along the edges of the microstructure

new RVE is not straight forward since particles are cut by the boundaries of the RVE. Therefore, one-point statistical correlation was used to calculate the volume fraction of the newly generated microstructure with the RVE by dropping random point in the microstructure to determine the probability of the point being inside the microstructure. The microstructure of a RVE with cut particles is shown in Fig. 5.7. The maximum volume fraction of microstructures generated using the RVE rises to $\sim 74\%$ for a system with 2×10^5 particles

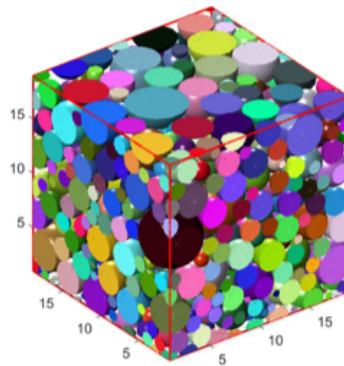


Fig. 5.7.: RVE generated by cutting particles across the edges

5.4 Summary of Algorithms to Develop Ultrapacked Microstructures

It is clear that the use of MDFS and the RVE is efficient in packing particles within a container. The algorithms developed in this study were capable of generating microstructures with volume fraction of $\sim 74\%$, which is in line with the packing in commercially used TIMs but is greater than that achieved in other microstructure simulations reported in the literature. The summary of the maximum volume fraction reached using various Random Sequential Addition based algorithms is tabulated in Table 5.1.

Table 5.1.: Summary of Random Sequential Addition based Algorithms

Algorithm	ϕ_{max} ($N_p \approx 10^4$)	ϕ_{max} ($N_p \approx 2 \times 10^4$)	ϕ_{max} ($N_p \approx 5 \times 10^4$)	ϕ_{max} ($N_p \approx 10^5$)	ϕ_{max} ($N_p \approx 2 \times 10^5$)
DFS	43%	53%	58%	61%	
DFS-Mixing	40%	44%	50%	54%	
MDFS	48%	58%	63%	67%	68%
MDFS-Mixing	43%	53%	60%	64%	
MDFS (RVE)	69%	70%	70%	73%	74%

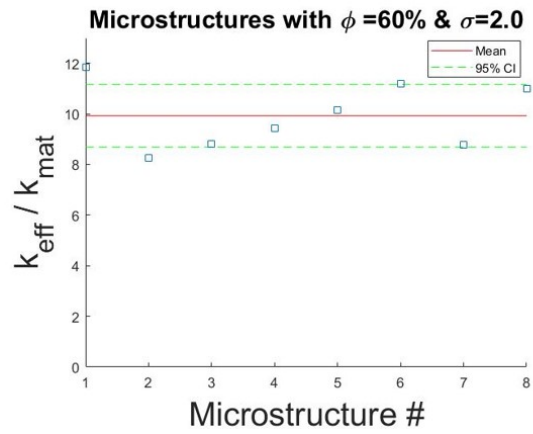
Having generated ultra-packed microstructures, the next step is evaluate the effective properties of the material using the random network model. This as described next.

5.5 Evaluation of Effective Properties of Ultrapacked Microstructures

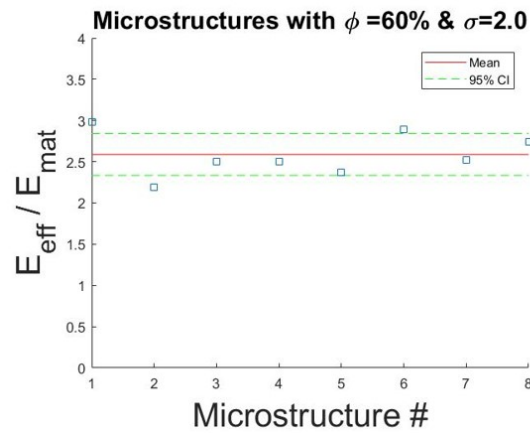
The microstructures generated as described in Sec.5.3 were evaluated using the Extended Random Network Model as described in Sec.3.3. In order to evaluate the

effective properties at increasing volume fractions, five sets of microstructures with a fixed value of volume fraction and polydispersity (characterized by the mean=1 and standard deviation=0.7 of the lognormal distribution of particle radii) was generated and evaluated as shown in Fig. 5.8. As an illustrative example, a system of aluminum particles ($k_p = 237$ W/m-K and $E_p = 70GPa$) in epoxy matrix material ($k_m = 0.3$ W/m-K and $E_m = 4GPa$) was simulated using microstructures with varying volume fractions. The values of normalized effective conductivity and effective elastic modulus are plotted in Fig. 5.9. It can be seen that values of effective properties are in close agreement with each other for the five microstructures.

In order to evaluate the effect of variation in polydispersity, eight sets of microstructures were generated for a fixed value of volume fraction, mean and standard deviation of the particle distribution. The mean value of radii was fixed to be 1 and the standard deviation was varied from 0.1 – 2.5. As shown in Fig. 5.10, there is a slight variation in the values of effective properties for a fixed value of volume fraction, particle size mean and standard deviation. This is attributed to the calculation of standard deviation which corresponds to the particle distribution of the original container (and not the RVE). However, the variation of the effective properties with polydispersity is found to be a second order effect as shown in Fig 5.8 in comparison to the effect of the volume fraction.

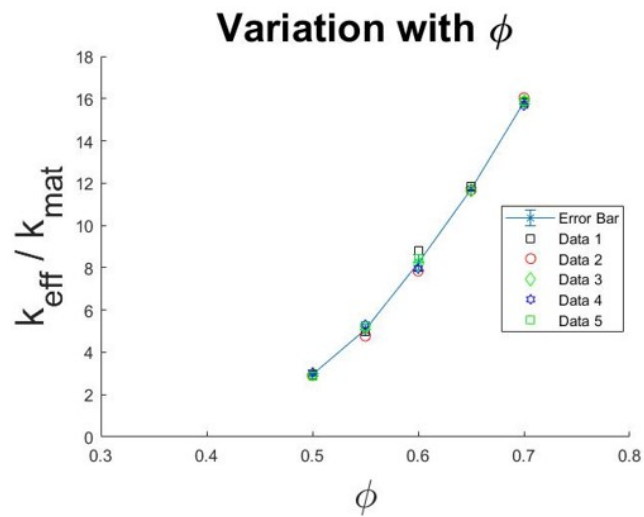


(a)

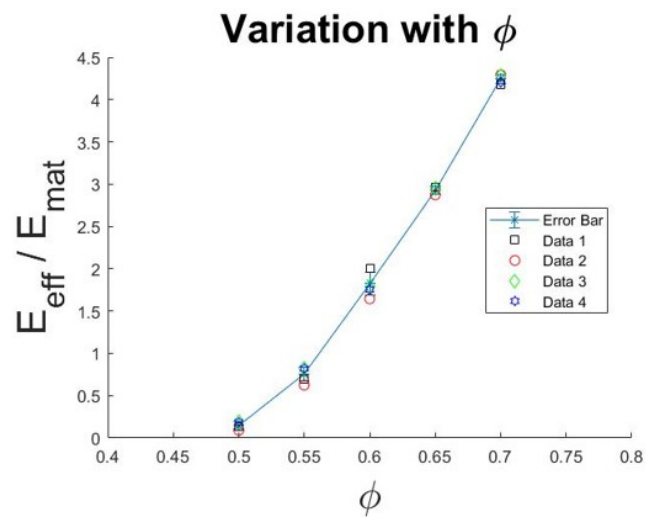


(b)

Fig. 5.8.: Variation of Effective Properties (a) Effective Conductivity (b) Effective Elastic Modulus

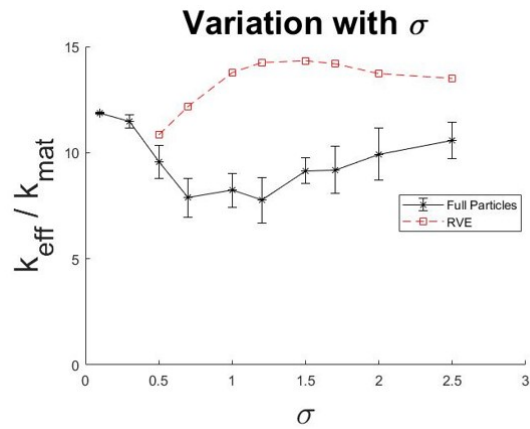


(a)

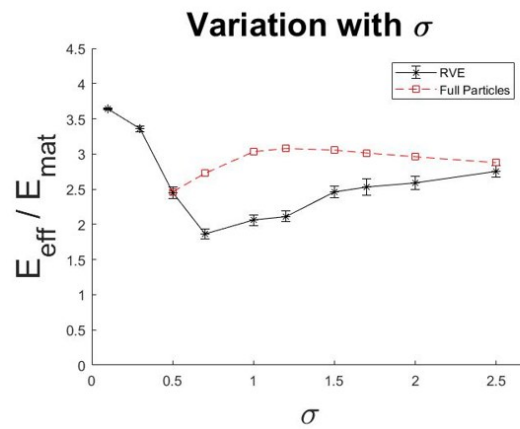


(b)

Fig. 5.9.: Variation of Effective Properties with volume fraction. Five random microstructures were generated at each volume fraction (a) Effective Conductivity (b) Effective Elastic Modulus



(a)



(b)

Fig. 5.10.: Variation of effective properties with polydispersity (a) effective conductivity (b) effective elastic modulus

6. CONCLUSIONS AND FUTURE WORK

6.1 Conclusions

Optimization and heuristic algorithms were evaluated in order to generate microstructures with ultrapacked filler particles. It was observed that both the non-linear programming algorithms and heuristic methods such as Drop-Fall-Shake could reach volume fraction of around 60% considering lognormally distributed full spheres in a box configuration. However, within a Representative Volume Element of the simulated container, with 2×10^5 particles such that the spherical particles cut across the edges, a maximum volume fraction of 74% could be reached. The Tables 4.2 and 5.1 summarize the results of Optimization Techniques and Heuristic Algorithms to generate microstructures. The method of considering a RVE with particles cutting across the edges was found to be the most efficient algorithm to generate ultrapacked cubic microstructures as shown in Fig. 6.1. The Random Network Model was extended to evaluate the RVE with partially cut particles. Thus realistic simulations of Thermal Greases were performed by generating microstructures and evaluating their effective properties.

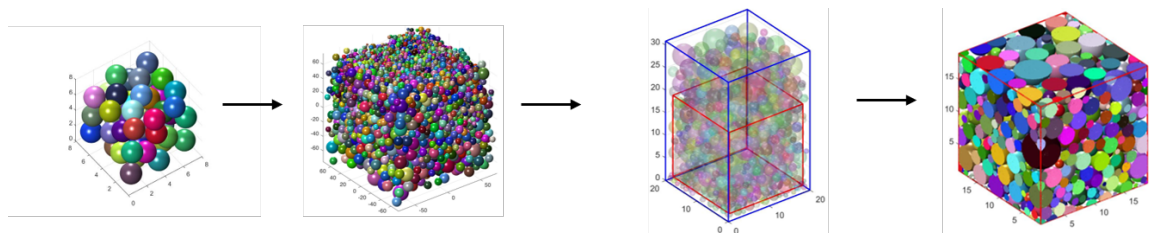


Fig. 6.1.: Microstructures generated with various algorithms

6.2 Future Work

The mathematical formulation of minimizing the gap between spheres can be extended to calculating the shortest distance between ellipsoids. Using this formulation, the optimization algorithms can be used to generate microstructures with ellipsoidal particles. The Random Network Model can be modified in order to capture the inter-particle interactions between ellipsoids in order to evaluate the effective properties of Thermal Greases with ellipsoidal particles.

REFERENCES

REFERENCES

- [1] M. Yovanovich and E. Marotta, “Thermal spreading and contact resistances,” *Heat Transfer Handbook*, vol. 1, pp. 261–394, 2003.
- [2] R. Prasher, “Thermal interface materials: historical perspective, status, and future directions,” *Proceedings of the IEEE*, vol. 94, no. 8, pp. 1571–1586, 2006.
- [3] C. Zweben, “Advances in composite materials for thermal management in electronic packaging,” *Jom*, vol. 50, no. 6, pp. 47–51, 1998.
- [4] E. Marotta and L. Fletcher, “Thermal contact conductance of selected polymeric materials,” *Journal of Thermophysics and Heat Transfer*, vol. 10, no. 2, pp. 334–342, 1996.
- [5] S. Mirmira, E. Marotta, and L. Fletcher, “Thermal contact conductance of adhesives for microelectronic systems,” *Journal of thermophysics and heat transfer*, vol. 11, no. 2, pp. 141–145, 1997.
- [6] P. Zhou and K. E. Goodson, “Modeling and measurement of pressure dependent junction-spreader thermal resistance for integrated circuits,” *ASME-PUBLICATIONS-HTD*, vol. 369, pp. 51–58, 2001.
- [7] S. Torquato, *Random heterogeneous materials: microstructure and macroscopic properties*. Springer Science & Business Media, 2013, vol. 16.
- [8] W. Yu, H. Xie, L. Yin, J. Zhao, L. Xia, and L. Chen, “Exceptionally high thermal conductivity of thermal grease: synergistic effects of graphene and alumina,” *International Journal of Thermal Sciences*, vol. 91, pp. 76–82, 2015.
- [9] L. Pournin, T. M. Liebling, and A. Mocellin, “Molecular-dynamics force models for better control of energy dissipation in numerical simulations of dense granular media,” *Physical Review E*, vol. 65, no. 1, p. 011302, 2001.
- [10] S. Kanuparthi, G. Subbarayan, T. Siegmund, and B. Sammakia, “An efficient network model for determining the effective thermal conductivity of particulate thermal interface materials,” *IEEE Transactions on Components and Packaging Technologies*, vol. 31, no. 3, pp. 611–621, 2008.
- [11] J. C. Maxwell, *A treatise on electricity and magnetism*. Clarendon press, 1881, vol. 1.
- [12] L. Rayleigh, “Lvi. on the influence of obstacles arranged in rectangular order upon the properties of a medium,” *The London, Edinburgh, and Dublin Philosophical Magazine and Journal of Science*, vol. 34, no. 211, pp. 481–502, 1892.

- [13] D. R. McKenzie, R. McPhedran, and G. Derrick, "The conductivity of lattices of spheres-ii. the body centred and face centred cubic lattices," *Proc. R. Soc. Lond. A*, vol. 362, no. 1709, pp. 211–232, 1978.
- [14] D. Hasselman and L. F. Johnson, "Effective thermal conductivity of composites with interfacial thermal barrier resistance," *Journal of composite materials*, vol. 21, no. 6, pp. 508–515, 1987.
- [15] D. Bruggeman, "Dielektrizitätskonstanten und leitfähigkeiten der mischkörper aus isotropen substanzen," *Ann. Phys.(Leipzig)*, vol. 24, pp. 636–664, 1935.
- [16] A. G. Every, Y. Tzou, D. Hasselman, and R. Raj, "The effect of particle size on the thermal conductivity of zns/diamond composites," *Acta Metallurgica et Materialia*, vol. 40, no. 1, pp. 123–129, 1992.
- [17] A. Devpura, P. E. Phelan, and R. S. Prasher, "Percolation theory applied to the analysis of thermal interface materials in flip-chip technology," in *Thermal and Thermomechanical Phenomena in Electronic Systems, 2000. ITherm 2000. The Seventh Intersociety Conference on*, vol. 1. IEEE, 2000, pp. 21–28.
- [18] D. Natekar, X. Zhang, and G. Subbarayan, "Constructive solid analysis: a hierarchical, geometry-based meshless analysis procedure for integrated design and analysis," *Computer-Aided Design*, vol. 36, no. 5, pp. 473–486, 2004.
- [19] X. Zhang, M. Rayasam, and G. Subbarayan, "A meshless, compositional approach to shape optimal design," *Computer methods in applied mechanics and engineering*, vol. 196, no. 17-20, pp. 2130–2146, 2007.
- [20] S. Kanuparthi, M. Rayasam, G. Subbarayan, B. Sammakia, A. Gowda, and S. Tonapi, "Hierarchical field compositions for simulations of near-percolation thermal transport in particulate materials," *Computer Methods in Applied Mechanics and Engineering*, vol. 198, no. 5-8, pp. 657–668, 2009.
- [21] P. K. Vaitheeswaran and G. Subbarayan, "Estimation of effective thermal and mechanical properties of particulate thermal interface materials by a random network model," *Journal of Electronic Packaging*, vol. 140, no. 2, p. 020901, 2018.
- [22] G. K. Batchelor and R. O'brien, "Thermal or electrical conduction through a granular material," *Proc. R. Soc. Lond. A*, vol. 355, no. 1682, pp. 313–333, 1977.
- [23] B. Dan, B. G. Sammakia, G. Subbarayan, and S. Kanuparthi, "An improved efficient network model for determining the effective thermal conductivity of particulate thermal interface materials," *Journal of Electronic Packaging*, vol. 135, pp. 031 003–031 003–8, 2013.
- [24] T. C. Hales, "Historical overview of the kepler conjecture," in *The Kepler Conjecture*. Springer, 2011, pp. 65–82.
- [25] S. Torquato, T. M. Truskett, and P. G. Debenedetti, "Is random close packing of spheres well defined?" *Physical review letters*, vol. 84, no. 10, p. 2064, 2000.
- [26] G. N. Vanderplaats, "Multidiscipline design optimization," *Applied Mechanics Reviews*, vol. 41, no. 6, pp. 257–262, 1988.

- [27] S. G. Nash and J. Nocedal, “A numerical study of the limited memory bfgs method and the truncated-newton method for large scale optimization,” *SIAM Journal on Optimization*, vol. 1, no. 3, pp. 358–372, 1991.
- [28] J. Nocedal and S. J. Wright, *Nonlinear Equations*. Springer, 2006.
- [29] R. Fletcher and C. M. Reeves, “Function minimization by conjugate gradients,” *The computer journal*, vol. 7, no. 2, pp. 149–154, 1964.
- [30] J. C. Gilbert and J. Nocedal, “Global convergence properties of conjugate gradient methods for optimization,” *SIAM Journal on optimization*, vol. 2, no. 1, pp. 21–42, 1992.
- [31] R. Andreani, E. G. Birgin, J. M. Martínez, and M. L. Schuverdt, “On augmented lagrangian methods with general lower-level constraints,” *SIAM Journal on Optimization*, vol. 18, no. 4, pp. 1286–1309, 2007.
- [32] ———, “Augmented lagrangian methods under the constant positive linear dependence constraint qualification,” *Mathematical Programming*, vol. 111, no. 1-2, pp. 5–32, 2008.
- [33] L. Smith and P. Midha, “A computer model for relating powder density to composition, employing simulations of dense random packings of monosized and bimodal spherical particles,” *Journal of materials processing technology*, vol. 72, no. 2, pp. 277–282, 1997.
- [34] *ROSS: Double Planetary Mixer*, May, 2015 (accessed May, 2018), <https://www.ceramicindustry.com/articles/94720-ross-double-planetary-mixer>.
- [35] M. Poux, P. Fayolle, J. Bertrand, D. Bridoux, and J. Bousquet, “Powder mixing: some practical rules applied to agitated systems,” *Powder Technology*, vol. 68, no. 3, pp. 213–234, 1991.